Waste heat recovery for lunar applications of a solid oxide electrolyser

Masteroppgave i Energiteknologi

Termiske Maskiner

Torstein Ragnhildson Storaas

Universitetet i Bergen

Geofysisk institutt

Høgskulen på Vestlandet

Institutt for maskin- og marinfag

Desember 2023

Waste heat recovery for lunar applications of a solid oxide electrolyser

Torstein Ragnhildson Storaas

University of Bergen

Faculty of Mathematics and Natural Sciences

Geophysical Institute

5020 Bergen, Norway

Department of Mechanical and Marine Engineering

Western Norway University of Applied Sciences

5063 Bergen, Norway

December 2023

Universitetet i Bergen (UiB)

Det matematisk-naturvitenskapelig fakultet

Geofysisk institutt

Allégaten 70

5020 Bergen, Norge

Høgskulen på Vestlandet

Fakultet for Ingeniør- og Naturvitskap

Institutt for maskin- og marinfag

Inndalsveien 28

5063 Bergen, Norge

Norsk tittel:	Gjenvinning av spillvarme for bruk ved en fastoksidelektrolysør på månen
Author(s), student number:	Torstein Ragnhildson Storaas, MAF012
Study programme:	Master in Energy, Thermal machines
Date:	20th December 2023
Supervisors:	Norbert Lümmen, HVL
	Richard J. Grant, HVL
	Ivar Wærnhus, Clara Venture Labs
Assigned by:	Clara Venture Labs
Contact person:	Ivar Wærnhus
Antall filer levert digitalt:	1/One

Preface

This master thesis has been written as part of the Master in Energy, Thermal machines. This program is a collaboration between the University in Bergen (UiB) and Western Norway University of Applied Sciences (HVL). The thesis was also written in collaboration with Clara Venture Labs to support their ongoing investigation in solid oxide electrolysis for space applications.

Firstly, I want to extend a big thanks to my HVL supervisors, Associate Professor Norbert Lümmen and Professor Richard J. Grant for their invaluable guidance, feedback and never-ending Star Trek quotes.

I would also like to thank Ivar Wærnhus for introducing me to Clara Venture Labs' exciting research on the topic of lunar solid oxide electrolysers.

A special thanks to Dan Shanker and the people of Aud 15.

And most of all I want to thank my family. My parents for countless hours of babysitting, their support and encouragement. Ida, and our children for their patience, support, and love.

Abstract

In an effort to make space exploration more sustainable the space industry looks to In-Situ Resource Utilisation (ISRU) as a possible way to lower the cost. With confirmed findings of water ice on the south pole of Earth's moon oxygen extraction with the help of Solid Oxide Electrolysis (SOE) is being investigated. SOE is a high temperature electrolysis technology with a high tolerance for impurities in its fuel stream. This makes SOE a promising technology for use in lunar ISRU production of oxygen. As an implication of its high operating temperature, thermal management is an important factor in lowering the overall energy demand of the electrolysis.

This report will investigate the waste heat recovery potential in the product gases from an SOE intended for oxygen production on the Moon. The SOE has an assumed electric power consumption and mass of approximately 13 kW and 26 kg respectively. Heat exchangers are investigated as a solution to recover the high temperature thermal energy in the product gases from the SOE in order to preheat steam that is supplied to it.

The commercially available design program Aspen Exchange Design and Rating (EDR) is used to design and compare different types and configurations of heat exchangers.

The results show that there is sufficient thermal energy to warrant the implementation of waste heat recovery. When using plate heat exchangers results show estimated power savings of between 1.3 kW and 1.5 kW depending on the size and configuration of the heat exchanger chosen.

The different configurations of the plate heat exchangers did not impact the amount of recovered heat in a meaningful way indicating that other considerations should be made when deciding on the design. The results for a configuration using a three-stream plate fin heat exchanger were unconclusive.

The mass flows of ca. 3 kg steam per hour for the specific SOE system under investigation were close to the lower mass flow limit of Aspen EDR. For further and more detailed investigations the use of a heat exchanger design software developed for such low mass flows is recommended.

Sammendrag

I et forsøk på å gjøre utforskning av verdensrommet mer økonomisk bærekraftig, ser romfartsindustrien til In-Situ Resource Utilisation (ISRU) som en mulig måte å redusere kostnadene på. Med bekreftede funn av vanninnholdig is på Sørpolen av jordens måne, undersøkes oksygenutvinning ved hjelp av en fastoksidelektrolysør (SOE). SOE er en høytemperatur elektrolyseteknologi med høy toleranse for urenheter i drivstoffstrømmen. Dette gjør SOE til en lovende teknologi for bruk i ISRU-produksjon av oksygen på månen. Som en implikasjon av den høye driftstemperaturen er spillvarmegjenvinning en viktig faktor for å senke det totale energibehovet til elektrolysøren.

Denne rapporten vil undersøke gjenvinningspotensialet for spillvarme i produktgassene fra en SOE beregnet for oksygenproduksjon på månen. SOE-enheten har et antatt elektrisk kraftbehov og masse på henholdsvis ca. 13 kW og 26 kg. Varmevekslere undersøkes som en løsning for å gjenvinne høytemperatur termisk energi i produktgassene fra SOE-enheten for å forvarme damp som tilføres den.

Det kommersielt tilgjengelige varmevekslerdesignprogrammet Aspen Exchange Design and Rating (EDR) brukes til å designe og sammenligne ulike typer og konfigurasjoner av varmevekslere.

Resultatene viser at det er tilstrekkelig termisk energi til å rettferdiggjøre implementering av spillvarmegjenvinning. Ved bruk av platevarmevekslere viser resultatene estimerte effektbesparelser på mellom 1,3 kW og 1,5 kW, avhengig av størrelsen og konfigurasjonen til den valgte varmeveksleren.

De forskjellige konfigurasjonene av platevarmevekslerne påvirket ikke mengden gjenvunnet varme på en meningsfull måte, noe som indikerer at andre hensyn bør tas når man bestemmer seg for design. Resultatene for en konfigurasjon basert på en tre-strøm-platefinnevarmeveksler var ikke entydige.

Massestrømmene på ca. 3 kg damp per time for det spesifikke SOE-systemet som ble undersøkt, var nær den nedre massestrømgrensen for Aspen EDR. For videre og mer detaljerte undersøkelser anbefales bruk av en programvare for varmevekslerdesign utviklet for slike lave massestrømmer.

Table of contents

Nomenclature

COP	Coefficient Of Performance
ESA	European Space Agency
HHX	Hydrogen Heat eXchanger
HP-SOC	High pressure electrolyser development for exploration surface missions
ISRU	In Situ Resource Utilization
LCROSS	Lunar Crater Observation and Sensing Satellite
LEO	Low Earth Orbit
MOXIE	Mars Oxygen In-Situ Utilization Experiment
NASA	National Aeronautics and Space Administration
OHX	Oxygen Heat eXchanger
PEL	Peaks of Eternal Light
PHX	Plate Heat eXchanger
PFHX	Plate Fin Heat eXchanger
PSRs	Permanently Shadowed Regions
PV	Photo Voltaic
SOC	Solid Oxide Cell
SOE	Solid Oxide Electrolysis

1. Introduction

The space industry is rapidly growing. Not so many years ago launching anything to orbit was something only achieved by superpowers. Now this happens on a regular basis by both countries and private companies alike. In 10 years, the number of objects launched to space have increased by 18,500 % [1]. This influx of competition has led to lower prices both for access to space and other related services. This has again led to more companies entering the market fuelling the rapidly growing space industry.

NASA has launched a new space programme called Artemis, together with several other partnering countries. The Artemis programme aims to establish a permanent settlement on Earth's moon and use this as a steppingstone for further exploration of Mars and beyond [2].

The Moon can work as a suitable training ground for future Mars expeditions as the relatively close proximity to Earth makes resupply and rescue missions fairly easy. While the Apollo 11 mission to the Moon lasted 8 days, a round trip mission to Mars would take approximately 3 years [3]. This means that a Mars mission needs to be as self-sustaining as possible; as it might take over a year for a resupply mission to arrive, depending on launch windows.

Even though the price of launching mass from Earth has declined in recent years, it is still far from being either economically or environmentally sustainable to rely solely on supplies from Earth. In situ resource utilisation (ISRU) can play an important role in lowering the cost of building and sustaining a lunar outpost. It is also important to be as self-sufficient as possible as humans venture further into the solar system. As the distance from Earth increases, the more complicated and costly resupply missions become. It is also a matter of safety, as relaying solely on resupply missions will make the crew heavily reliant on regular launches from Earth.

The lunar surface is covered with layer of a rock called Regolith. It varies in size from large boulders to fine dust (averaging 45-100 μm). It can be used to build structures using additive manufacturing or simply cover existing buildings to provide thermal insulation and radiation protection [4], [5].

Water ice has been located in large quantities in permanently shadowed regions (PSRs) on both the south and north poles of the Moon. The biggest concentrations are found in craters in the south pole [6]. It is due to the altitude of the sun, i.e. the sun angle, striking the poles coupled with the small lunar obliquity (causing little variation in the path of the sun for the lunar summer and winter) that PSRs are possible on the lunar poles. It also allows permanently unshaded regions to exist on certain elevated topographical features such as the rims of craters, which are known as peaks of eternal light (PEL). In PSRs the temperature can be as low as -250°C. This means that a lot of heat will be required to melt the ice to separate it from other volatiles and gases that it might be mixed with. Locating PSRs close to PELs will be an important factor in identifying locations for future ISRU operations. This can provide both large amounts of solar power and a proximity to water.

Shackleton crater provides both a proximity to PELs on its rim and PSR in its crater. This has made it one of the front runners for a future lunar base location [7]. In Figure 1, both the brightly lit crater rim and the crater floor can be seen. The picture is made possible by combining pictures taken using two cameras with different light-sensitivity.

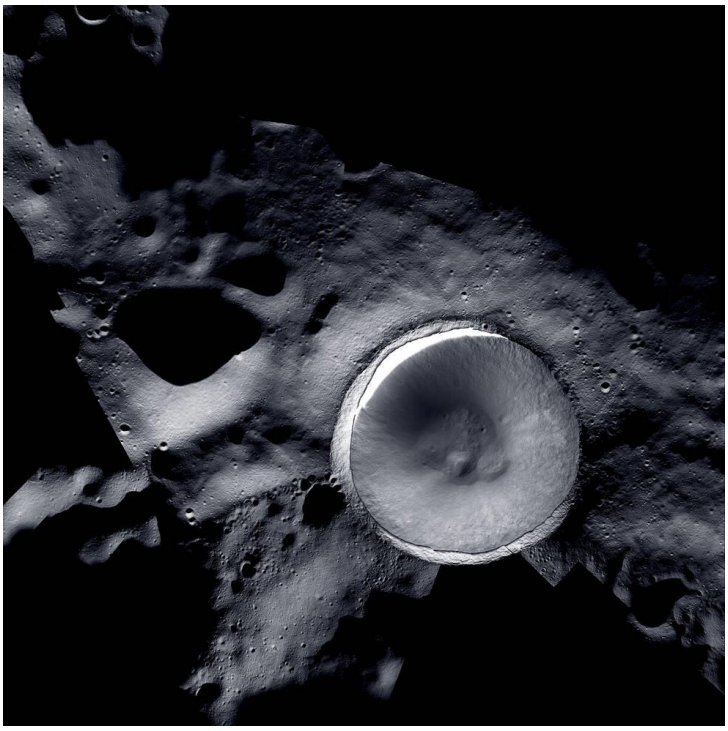

Figure 1. A picture of Shackleton Crater combining images from Lunar Reconnaissance Orbiter (LROC) and ShadowCam [8].

Beside sunlight for energy, water ice is perhaps the top target for ISRU because of its many uses. It can be used both for consumption, cleaning and radiation protection; but also split into oxygen and hydrogen with the help of electrolysis. This can be used for energy storage in combination with a fuel cell, as rocket fuel, as well as supplying a life support system with oxygen. There are several ideas as to how lunar ice can be mined [9]. One approach is mining in the most classical sense whereby regolith is excavated containing ice from the ground and then extracting the water, typically by heating it. Another proposed solution is the sublimation method where the ground containing ice deposits is heated to cause sublimation [10]. This causes the steam to rise up to the ground where it is collected.

Solid Oxide Electrolysis (SOE) is a high temperature electrolysis method which can be used for production of oxygen and hydrogen in a lunar environment. The high operating temperature of the SOE leads to a high tolerance for impurities in its feedstock when compared with other electrolysis methods [11]. This is well suited for the water ice found on the moon as it is assumed to have a high amount of methane [12]. Another advantage of the SOE is the ability to greatly improve their overall efficiency with effective thermal management. This means that an effective use of heat recuperation combined with the potential use of external waste heat can lower the need for electrical energy. The lunar environment with its lack of atmosphere also

makes it difficult to dispose of excess heat. An added benefit of heat recouperation is that it reduces the need for radiators for cooling.

SOE technology has already been successfully demonstrated with the Mars Oxygen In-Situ Utilization Experiment (MOXIE) where a SOE located on the Mars rover Perseverance produced oxygen from the Martian atmosphere by splitting CO_2 into CO and O_2 [13].

In 2020 the European Space Agency (ESA) launched a research project called High Pressure Electrolyser Development for Exploration Surface Missions (HP-SOC) which was awarded to Clara Venture Labs and Centre of Research Technology Hellas (CERTH). The project aims to investigate the use of high-pressure Solid Oxide Electrolysers (SOE) for oxygen and fuel production in an ISRU setting on the Moon and Mars [14].

This thesis aims to support Clara Ventures Labs' research project by investigating how heat can be recuperated to reduce the energy demand of the SOE. It will investigate what type of heat exchanger is most suitable to work in the harsh lunar conditions and how much heat it is possible to recover. It will specifically concentrate on recuperating heat from the hydrogen and oxygen exhaust coming from the SOE and use this to heat the incoming steam fuel.

1.1 Aim

The aim of this thesis is to investigate the potential for waste heat recovery of a Solid Oxide Electrolysis (SOE) system intended for lunar In Situ Resource Utilisation (ISRU), both as a means of thermal management and increasing efficiency.

1.2 Objectives

Identify the largest amount of heat that can be practically recuperated.

Identify the most suitable heat exchanger design.

Investigate how different operating pressures impact the heat exchanger design.

1.3 Structure

The following five chapters are structured as follows:

Chapter 2 will provide brief background to understand reasons behind the design decisions.

Chapter 3 will describe what will be simulated and how.

Chapter 4 present the results from the simulations.

Chapter 5 discusses findings in both the simulations and the literature study.

Chapter 6 provides a summary of the most important findings as well as suggestions for further work.

2. Background

The following subsections will provide background information on leading factors that will guide the requirements and design process for a heat exchanger suitable to operate in a lunar environment in conjunction with a Solid Oxide Electrolyser (SOE).

2.1 The lunar environment

The Moon offers extreme conditions with temperatures up to 120˚C during the lunar day in equatorial regions. During the lunar night, which lasts for almost 14 Earth days, the temperature falls to -130˚C. For any practical case there is no atmosphere, making it difficult to remove excess heat from equipment such as devices and astronauts' space suits. This implies that systems designed for this environment should rely as little as possible on external heat and cold flows to maintain their operating temperature. If items are being exposed to either sunlight or lack thereof, either the hot or cold streams become a valuable resource. It is then possible to create synergy effects using heat released by equipment to keep other equipment from freezing. With this, the hot and cold streams are kept within the system boundary, minimising the need for external cooling and heating.

The Moon is covered by a layer of rock and dust called regolith, typically 4-5 m thick [15]. It is the result of eons of constant impact of meteors and of particles from the sun. The regolith varies in size from large boulders to microscopic dust particles smaller than 10 μm. Due to the lack of wind and liquid flows, the regolith does not erode over time and smooth out like on Earth. Instead, the material has a fractured surface with sharp edges. The regolith attaches to most surfaces due to a positive static electric charge caused by solar radiation. The sharp edges make the dust abrasive, which can cause damage to equipment [16].

In recent years, large amounts of water ice have been detected in the Moon's polar regions [6]. This ice is located in permanently shadowed regions (PSR). These are areas of the Moon that do not receive direct sunlight. Such PSRs are often located in impact craters around the poles. Due to the low angle of the sun, the crater floor never sees direct sun light. The temperature in these PSRs can be as low as -250˚C. The cold temperatures keep the water ice from evaporating into space. Another implication of the sun's low angle at the poles is that elevated terrain may experience prolonged periods of direct sunlight, some up to 85% of the lunar year [17]. These regions are referred to the somewhat incorrectly name of Peaks of Eternal Light (PEL). These can provide locations for harvesting solar energy with Photo Voltaic (PV) solar cells with close to uninterrupted exposure to sunlight.

When planning for a future lunar base, proximity to both PSRs and PELs will be beneficial. This will enable high power production from solar cells as well as the possibility to mine water ice from the PSR. Several such sites exist, with Shackleton crater likely to be the most widely known.

The Moon has the same solar irradiance as the Earth at 1361 W/m^2 [18]. The lack of atmosphere does, however, make PV solar panels more efficient overall compared to Earth. This is due to

the Earth's atmosphere absorbing some of the sun light which makes it impossible to achieve the theoretical 1361 W/m^2. PV solar panels can achieve as high power to mass values as 350 W/kg; although, this is for the panels themselves. Additional infrastructure and inefficiencies downstream will make this value smaller, some estimates place this at 170 W/kg [21]. Nuclear power will not need power storage solutions at the same scale as PV solar panels. This is because this technology is not dependent on sunlight to produce power. When considering the power to weight ratio of nuclear power sources, estimates lie between 6.5 W/kg and 42 W/kg depending on power output and mobility [19], [20], [22], which is considerably lower than PV solar panels. However, a benefit of nuclear power is that it will produce large quantities of waste heat that can potentially be utilised for other purposes other than power production [23].

National Aeronautics and Space Administration (NASA) has launched the Artemis Program, which plans to bring humans back to the lunar surface for the first time in over 50 years. With this programme NASA, with partnering countries, aims to extend human presence on the moon by establishing a base camp on the lunar south pole [2]. This can later be used as a steppingstone for further venturing into the solar system. To make this endeavour and space exploration at large more economically sustainable, In-Situ Resource Utilisation (ISRU) has become an important area of interest.

2.2 In-Situ Resource Utilisation (ISRU)

In-Situ Resource Utilisation (ISRU) is a term used when resources are sourced locally. It is most commonly used to refer to space related operations. This is typically done in an effort to lower the amount of resources, and therefore mass, needed to be brought from Earth.

With the commercialisation of spaceflight many new entities have entered the launch business. This has led to the development of new and more cost-effective ways to send mass into orbit around Earth and beyond [24]. Even with the introduction of reusable rockets, the price still remains relatively high. Costs are ranging from 1500 $/kg on heavy rockets (SpaceX Falcon Heavy) to 23,100 $/kg for a small, dedicated launch vehicle (Rocket Lab Electron) to Low Earth Orbit (LEO) [25]. This makes minimizing the mass-to-orbit an important metric to lower the overall cost of missions.

In the case of the Moon several potential ISRU targets exists. The lunar regolith has many potential uses and applications in an ISRU setting. Proposals suggest covering a lunar base with a layer of regolith in an effort to provide protection from meteors and radiation as well as thermal insulation [26]. Other studies suggest using the regolith in combination with additive manufacturing to construct different structures [5]. Based on recent observations by the Chandrayaan-1 and LRO space craft it is estimated that 600 million tonnes of water ice are located at the lunar poles [6]. This is however a conservative estimate, which is affected by radar strength and the ability of the radar radiation to penetrate deep into the ground. Estimates from the The Lunar Crater Observation and Sensing Satellite (LCROSS) mission suggests a water ice concentration of 5.6% ± 2.9% by mass present in the crater impacted. Measurements

of the composition of the water ice found can be seen in Table 1. It contains large amounts of hydrogen sulphide, ammonia and methane among others.

Table 1. Composition of water ice. This table is sourced from ref. [12].

Compound	% Relative to H_2O(g)
H_2O	100%
H_2S	16.75%
NH_2	6.03%
SO_2	3.19%
C_2H_4	3.12%
CO_2	2.17%
CH_3OH	1.55%
CH_4	0.65%
OH	0.03%

Water is a top priority for ISRU because of its many potential uses to support human missions. It can be used as consumables or be split into H_2 and O_2 with the help of electrolysis. The H_2 and O_2 can be used both as rocket fuel, energy storage in combination with a fuel cell, and the O_2 can be used in the life support system for breathing.

There are several concepts for water retrieval in the lunar regions proposed. The sublimation method envisions heating up lunar soil rich in water ice to cause the water to sublimate. It will then rise from the ground and can then be collected [10]. Another method is the more familiar strip mine approach, where ice containing regolith is collected by excavators and heated up to separate the water from the other materials [9].

The ice found in the PSRs has the same low temperature as its surroundings. This means that the ice could work as a heat sink for other equipment or processes. If the water is being electrolysed, the low temperature of the ice might be used in the liquefaction process of the H_2 and O_2 to save energy.

2.3 Solid Oxide Electrolysers (SOE)

A Solid Oxide Electrolyser (SOE) is a type of electrolyser using an oxide conducting ceramic as the electrolyte. This makes the device solid state, which is beneficial in harsh conditions like the ones experienced in a lunar environment. Another benefit with SOEs is the high operating temperature, typically between 600˚C and 1000˚C. This makes the SOE technology more resistant to the impurities found in the lunar water ice compared to alternative electrolysis methods like PEM and alkaline electrolysis. The high operating temperature does however also lead to several engineering difficulties associated with high temperatures [11].

To mitigate oxidation of the nickel-based electrodes a small amount of ca. 5% by mole of H_2 is introduced to the steam flow. This ensures a chemical environment that keeps the nickel reduced including at the inlet of the SOE.

The voltage needed to run the SOE varies depending on the conversion rate of the steam to H_2 and O_2. When the SOE approaches a 100% conversion rate, the voltage required increases drastically. To avoid the higher energy consumption SOEs will typically be run around 80% conversion rate.

When electrolysis is used to extract the O_2 from the water ice, a biproduct will be H_2. The H_2 is a valuable resource which can be used as fuel in a fuel cell and as rocket propellant. An advantage with the Solid Oxide Cell (SOC) is that it can work both as an electrolyser and a fuel cell. This way, a single setup can be designed for resource production, while it also possesses the ability to work in reverse to generate power. This will generate both power and heat, which will be in demand during the lunar night.

SOE is already a proven technology for ISRU. In 2021 Mars Oxygen In-Situ Resource Utilization Experiment (MOXIE) produced oxygen from CO_2 captured from the Martian atmosphere [27]. In this experiment located on the Mars rover Perseverance, a SOE produced oxygen at a rate of 6 g/h. This was done by splitting CO_2 into CO and O_2.

Electrolysis utilising SOCs can be run to be exothermic, endothermic, or thermoneutral depending on the voltage that is applied to the stack. Typically, SOEs are run in thermoneutral mode because the exothermic mode can impact the lifetime of the cell. The exothermic mode also requires a higher current and voltage, and therefore more power. Research suggests that an endothermic mode can be beneficial as this allows for the stack to operate with a lower current and increase its lifetime [28]. It will then however rely on external heat to operate. Effective thermal management is important to achieve high electric efficiency with SOE in all the operating modes, the difference is the direction of the heat flow [29], [30].

2.4 Project and system outline

ESA is currently investigating the potential for SOEs for future lunar and Martian ISRU with the programme High Pressure Electrolyser Development for Exploration Surface Missions (HP-SOC). ESA awarded Clara Venture Labs together with Centre of Research Technology Hellas (CERTH) with a research grant to further its development. The goal of the project is to develop an SOE to extract oxygen from lunar resources and atmospheric CO_2 on Mars.

Clara Venture Labs, previously named Christian Michelsen Research (CMR) Prototech, was founded in 1988 by Odd Dahl. The company is an early-stage venture lab focusing on developing industrial innovations within energy systems, advanced materials and other related fields.

HP-SOC is still in an early phase and is focusing on developing the technology to be suitable for a variety of missions. Therefore, few specifics are known regarding the target area and the environment for the SOE and ISRU operations. As seen in Section 2.1 the location chosen on the Moon has large implications on the design. If the location is in a Permanently Shadowed Region (PSR) cooling will likely not be a problem, and the high temperature product streams (H_2 and O_2) leaving the SOE will be seen as assets. If the location, on the other hand, is experiencing direct sunlight external cooling might be necessary and the relatively cold steam

flow might be utilised. As the largest concentrations of lunar ice are located in the polar areas this is the most likely environment for the ISRU operations. The study will investigate solutions which will be suitable for most applications and therefore focus on utilising the internal heat streams of the system.

The focus of this thesis is the lunar application of this project and therefore the fuel source is steam sourced from lunar water ice. It is assumed that the H_2O is extracted from the lunar regolith with the help of heat to support the phase shift into steam. To limit the scope of the investigations the system boundaries are set after the ISRU process. For the sake of simplicity, a temperature of 200˚C was chosen as the inlet temperature of steam for all pressures. This implies that there is an electric heater present between the boiler and the heat exchanger in order to super heat the steam. As the temperature of evaporation changes with different pressures, new inlet temperatures for the steam would have to be set for each operating pressure. ESA have specified that the HP-SOC target production is 50 g/min of oxygen and 6.3 g/min of hydrogen with a target operating pressure of 10 bar [31]. It is assumed that the SOE will have a power consumption of approximately 13 kW and a mass of 26 kg to achieve this output. During earlier phases of the project some challenges were however identified related to specifying such a high operating pressure. A range of pressures between 1 and 10 bar will be considered and investigated as part of the evaluation of the benefit and potential problems related to high heat exchanger operating pressures.

Elevating the temperature of the steam, referred to as the cold stream or flow, to as close to the operating temperature of the SOE as possible with the heat available from the O_2 and H_2 streams, referred to as the hot streams or flows, will be the overall objective. The hot streams initially hold the same temperature as the SOE's operating temperature at 820˚C.

This thesis will evaluate the possibility of using commercially founded design and simulation software to design heat exchangers for the hot and cold streams of the SOE system; i.e. not specialist simulation tools offering a bespoke space-grade solution. It is desirable to both minimise the need for external cooling and heating which can lead to both power and weight savings.

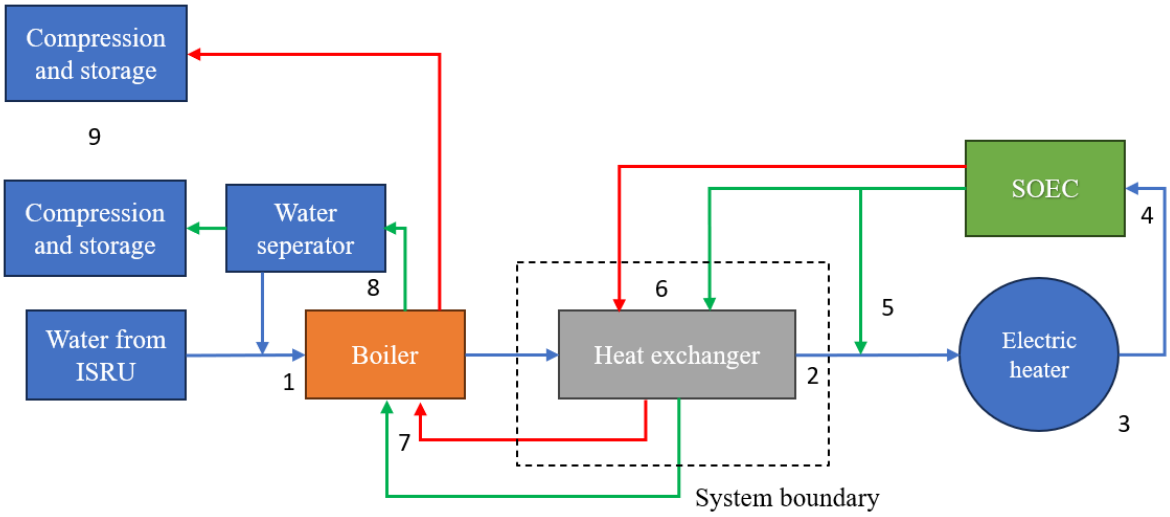

Figure 2.The schematics of the electrolysis system. The doted box outlines the defined system boundaries of this investigation. The green line represents the H_2/H_2O stream, the red line is the O_2 stream while the blue line is the steam flow. Explanation of the numbers is given in the text.

A flow diagram showing the mass flow of the system and the system boundary of this project can be seen in Figure 2. The explanation for the numbers in the figure is as follows:

1. Water enters the system, either as ice or liquid from an ISRU operation. In a boiler it is heated to 200˚C at constant pressure, which induces a phase change into superheated steam. The process will also include a pressurisation stage.

2. In a heat exchanger the steam is heated as close to 820˚C as practicable.

3. An electric heater ensures the cold stream reaches the intended temperature of 820˚C.

4. The steam enters the SOEC where it is split into O_2 and H_2.

5. The H_2 stream contains 80% mole fraction H_2 and 20% mole fraction steam. Some of the produced hydrogen is fed into the steam flow going into the electric heater to give the steam flow a 5% mole fraction H_2 concentration.

6. The H_2 and O_2 streams enter the heat exchanger at 820˚C.

7. It will not be practical to transfer all the heat in the heat exchanger as this would make it impractically large. Excess heat can therefore be used in the boiler.

8. The H_2 enters a water separator. The separated water is then fed back into the boiler.

9. The O_2 and H_2 are compressed and chilled for storage. This will produce more heat which potentially can be utilised in the ISRU process.

2.5 Gravitational effects on heat transfer and fluid flow

The gravitational forces of the Moon are about 1/6 of Earth gravity at 1.62 m/s^2. This can have some effects on the heat transfer and fluid flow with a reduction in buoyancy. Natural convective flow will be somewhat reduced due to the lower gravity, this this can however be treated as being insignificant as effects typically scales at $g^{1/4}$ compared to Earth [32]. Gravity affects the hydrostatic pressure where the low lunar gravity will decrease the static pressure. The forced convective flow in the heat exchangers will not be affected by the reduced gravity on the Moon because the governing equations do not depend on g [33].

2.6 Heat exchangers

There are many types of heat exchangers, all with the general goal of transferring heat between media without mixing them. Depending on what kind of medium the hot and cold streams are made up of different design are considered more effective. According to literature the three most common heat exchanger types when dealing with gas-to-gas heat transfer are shell and tube, plate and plate fin heat exchanger [34], [35]. Plate heat exchangers can achieve the same amount of heat transfer area as a shell and tube heat exchanger with only 20 – 30% the mass [36]. Since low mass is a critical design criterion when designing equipment for space flight, shell and tube heat exchangers will not be investigated further.

2.6.1 Plate heat exchanger (PHX)

A plate heat exchanger (PHX) consists of several, typically corrugated, plates sandwiched together. Plate heat exchanger typically refers to the most common plate-and-frame design which are made up of several plates sandwiched together by a frame. It is however also possible to join the plates together with brazing. This is sometimes referred to as a brazed plate heat exchanger. Additionally, plate fin heat exchangers are sometimes grouped into the broader plate heat exchanger term; they will however be covered in their own subsection in Section 2.6.2.

In a plate-and-frame design the plates are sealed with gaskets. This means that it is possible to separate the plates for cleaning, or to increase the capacity for larger streams or a higher heat recuperation. This is not something that will be feasible for this project. It could however be of some interest for a future project supporting a larger lunar base where maintenance would be possible.

The seals are however more prone to leakage when operating at high temperatures and pressures. For these applications the plates are typically joined by brazing or laser welding. When welding is used for the bonding, a more compact heat exchanger is typically achieved relative to when plate-and-frame design are used [34]; however, when the plates are welded together cleaning becomes more complicated. Therefor a brazed heat exchanger design will typically only be used for applications with low fouling. Fouling is a term used when particles get stuck inside the heat exchanger and the heat exchanger area is covered in foreign object debris, deteriorating the heat transfer. Plate heat exchangers are quite susceptible to this fouling

due to their narrow passages, which can lead to both large pressure drops and less effective heat transfer.

The streams entering the heat exchanger are routed to different sides of the plates. The plate heat exchanger is scalable by simply adding more plates. Depending on how the stream is routed, it is possible to create several passes of the streams. Alternatively, there can be one pass with several plates; increasing the heat transfer area, but not the residency time.

The plates of a plate heat exchanger come with various corrugations. This will greatly impact both the thermal and hydraulic performance. The most common corrugation is referred to as a chevron, seen in Figure 3. The angle and number of chevrons can vary depending on desired hydraulic traits.

Figure 3.. A single plate from a plate-and-frame heat exchanger with chevron corrugation. [35]

The corrugation in the plates induces turbulence to the flows as well as increasing structural integrity. The induced turbulence increases the heat transfer between the flows, whilst also increasing the pressure drop created by the plate heat exchanger.

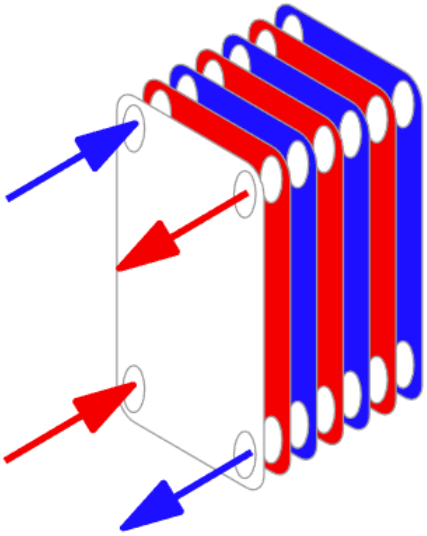

Figure 4. The flows of a plate heat exchanger can be seen. The blue plates represent the cold stream while the red represent the hot stream. [38]

In Figure 4 a schematic of a plate frame heat exchanger can be seen. The schematic would however be close to identical for a brazed plate heat exchanger as well. The red colour represents the hot stream while the cold stream is blue.

2.6.2 Plate fin heat exchanger (PFHX)

Plate Fin Heat Exchangers (PFHX) are typically compact, but still offer a large heat transfer area. This is due to the heat exchanger design. The construction is made up by corrugated fins sandwiched between flat plates. These fins are brazed to the flat plate, whilst the corrugated geometry serves to provide both extra heat transfer area and mechanical support. They also provide the added benefit of introducing turbulence to the flow. The fins come in several varieties, from plain, perforated and serrated among others [37]. The added heat transfer area provided by the fins is beneficial when operating with streams that have a low heat transfer coefficient. Therefore, PFHX are typically used for gas-to-gas applications [35], [39]. PHFX are suitable for a large variety of temperatures, typically limited by materials and bonding method. The bonding method used also affects the magnitude of the operating pressure the PFHX can withstand. With diffusion-bonded PFHX operating pressures as high as 200 bar have been achieved [35].

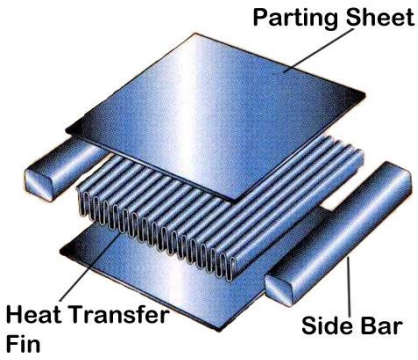

Figure 5. Plate fin heat exchanger with corrugated fins sandwiched between two plates. [40]

In Figure 5 a typical PFHX can be seen. The fins provide a significant increase in heat transfer area, this does however also add more material to the construction and therefore mass.

2.7 Material selection

When choosing a material to construct a heat exchanger to operate with a SOE several factors need to be taken into consideration. The heat exchanger will be subjected to the same high temperatures as the SOE. This means that the material for the heat exchanger transfer areas would need to withstand temperatures above 800˚C. The high temperatures in combination with steam and O_2 can also lead to oxidisation and corrosion while the presence of H_2 can lead to hydrogen embrittlement. This means that many considerations need to be taken into account when choosing a material for the heat exchanger.

Iron based alloys are often used for heat exchangers up to around 600˚C. When the temperature exceeds this value other metals are usually used due to corrosion issues and low tensile strength

at high temperatures [39]. For high temperature heat exchangers nickel-based superalloys are more commonly used. They offer a high temperature resistance as well as high tolerances for corrosion and high pressures. Inconel 625 offers a high resistance to temperature and good resistance to corrosion with the added benefit of being suitable for additive manufacturing [41].

Ceramics are often used for high temperature heat exchangers. They offer high temperature resistance and a high resistance to corrosion. However, they do not handle very high pressures well, are hard to seal, and have issues related to brittleness [37].

A high thermal conductivity is desirable, but because the heat transfering plates typically are very thin, this does not overly affect the overall heat transfer. The density of the material is more important when evaluating materials for space related use. If it is possible to lower the mass of the heat exchanger by using a lighter material, a heat exchanger with a larger heat transfer surface can be chosen. This will typically far outperform a heat exchanger using materials with higher thermal conductivity and density.

Table 2. Thermal conductivity and density of various metals.

	Thermal conductivity [W/m˚C]	Density [kg/m^3]
Stainless steel	17.6 [42]	7480 – 8000 [43]
Hastelloy	21.3 [42]	8940 [43]
Inconel 625	13.4-21.3 [44]	8440 [44]

In Table 2 the thermal conductivity and density of various metals used in heat exchangers are presented. The stainless steel and Hastelloy values for thermal conductivity are sourced directly from the simulation program used in Section 3.2. As thermal conductivity values are temperature dependent it is assumed that the numbers are averaged. The thermal conductivity for Inconel 625 is presented for the interval between 200-600˚C. Both Hastelloy and Inconel 625 can withstand the high temperatures experienced when operating in conjunction with a SOE. Inconel 625 has a slightly lower thermal conductivity than Hastelloy has. It does however have a slightly lower mass and the ability to be additively manufactured which could make it more suitable for a finale design.

3. Method

This chapter will describe the different heat exchanger configurations that will be investigated in this report. It will look at the reasoning behind how the software was used and difficulties encountered.

3.1 Defining the problem

The objective is to produce a constant stream of 50 g/min of oxygen (O_2). This is the only known mass flow, so the rest of the streams have to be calculated based on this. It is known that the SOE is operating at a conversion efficiency rate of 80% by mole, meaning that of the steam going into the electrolyser, 80% by mole is converted to H_2 and O_2. The remaining 20% by mole of unconverted steam exits together with the H_2 stream. This stream of 80% H_2 and 20% by mole steam will be referred to as simply the hydrogen stream, even though it is still part steam.

To calculate the rest of the mass flows based on the known O_2 stream, a molar analysis will have to be performed. First the mole flow in the oxygen stream has to be established by using

$$\dot{N}_{O_2} = \frac{\dot{m}}{M} \tag{1}$$

where $\dot{N}$ is the mole flow, $\dot{m}$ is the mass flow, and M is the mole mass of a given substance.

This provides the number of moles in the O_2 stream, which is the same amount of mole converted by the SOE. This does however not include the 20% unconverted mole in the form of steam leaving the SOE with the H_2. This can be identified with

$$\dot{N}_{\text{total}} = \frac{\dot{N}_{O_2}}{y_{O_2}} \tag{2}$$

where y_{O_2} is the mole fraction of oxygen. Dividing the amount of moles of pure oxygen in the stream by the percentage (in this case 80%) of the total stream the total mole flow of the stream can be identified.

Now that the total mole flow is established it is possible to determine both the mass flow of steam input and the mass flow of steam in the hydrogen stream. They are listed in Table 3.

Table 3. The mole flow and mass flow of the different streams.

Stream	$\dot{N}$ [mol/min]	$\dot{m}$ [g/min]	$\dot{m}$ [kg/h]
Oxygen (O_2)	1.56	50	3
Hydrogen (H_2)	3.13	6.3	0.38
Steam part of hydrogen stream	0.78	14.1	0.85
Hydrogen stream	3.91	20.4	1.22
Steam input mass flow	3.91	70.4	4.22

The objective is to design a heat recuperating system based on heat exchangers. The system boundaries are therefore set to only entail the heat exchangers as seen in Figure 2. The SOE operates at 820˚C, meaning that the hot streams of H_2 and O_2 exiting the SOE will hold the same temperature. The hot streams will therefore be set to 820˚C when they enter the system boundaries of this study. The cold stream is sourced from an undecided ISRU operation. It is unknown what specific process that will be used to extract the water from the lunar ice and what exit temperature this will produce. For the sake of this study the inlet temperature of the steam will be set to 200˚C. This is above the saturation temperature for all the investigated pressures to ensure that there are no phase changes present in the steam flow, even if the pressure drops because of the steam flow experiencing friction in the heat exchanger. It is important to receive directly comparable results in regard to thermal energy recovery across all the different operating pressures. Raising the steam temperature as close to 820˚C as practicable with a minimum increase in heat exchanger mass is the overall goal.

If no heat recuperation is used, an electric heater would need to be used to raise the temperature of the steam flow to 820˚C before entering the SOE. Using Equation 3, the thermal power in the various flows can be calculated. This was done by multiplying the specific enthalpy change by mass flow:

$$\dot{Q} = \dot{m}\Delta h \tag{3}$$

where Δh is the specific enthalpy difference between 820˚C and 200˚C of the different streams at the given pressure and $\dot{m}$ is the mass flow of the chosen stream. The specific enthalpy values seen in Table 4Table 6Table 6 are obtained in kJ/kg from Aspen. It should also be noted that the combined thermal energy in the hydrogen and oxygen streams are higher than what is needed to heat the steam to 820˚C. This indicates that it should be enough heat to reach the intended 820˚C of temperature for the steam. The only limiting factor will be how large the heat exchanger needs to be to achieve this.

Table 4. The thermal power of the different flows in the system, the value for the hydrogen stream is the combined value of 80% H_2 and 20% H_2O.

	Hydrogen	Oxygen	Steam
h_{820} [kJ/kg]	-4520	811	-11,760
h_{200} [kJ/kg]	-8275	164	-13,090
Δh [kJ/kg]	3755	647	1330
$\dot{m}$ [kg/h]	1.22	3.00	4.22
$\dot{Q}$ [kW]	1.27	0.54	1.56

Assuming the electric heater has a Coefficient Of Performance (COP) of 1, the power demand to bring the steam from 200°C to 820˚C in the case of no heat exchanger would be 1.56 kW.

To investigate how pressure affects the heat exchanger design, simulations will be made at 1, 5, 8 and 10 bar absolute. When referencing pressure in this report it is always to be considered as an absolute pressure, unless otherwise specified. The maximum allowable pressure loss in the heat exchangers was set to 0.1 bar, this was never exceeded and is therefore not mentioned in the results.

Due to the large cost of transporting mass to the lunar surface, keeping the mass as low as possible becomes a priority. This implies that the amount of recovered heat in the heat exchanger must be seen in relation to the size of the exchanger.

The low gravity of the Moon can theoretically impact the performance of a heat exchanger to some degree. The static pressure will be lower due to the lower gravity. In a heat exchanger of the sizes investigated here this will, however, be negligible. Natural convection is also affected by gravity; but as the flows in the heat exchanger will be of the forced convective type and turbulent, in an effort to increase heat transfer, this will not have any implications. Therefore, the analysis will be done without modification to the simulation program's gravitational constant.

3.2 Aspen Exchanger Design & Rating (EDR)

Aspen EDR is a design software for heat exchangers made by Aspentech. It is part of the AspenONE suite of programs. It works by suggesting heat exchangers based on inputs of mass flows and temperatures. When a specific heat exchanger is chosen it can simulate the performance of the selected heat exchanger.

Aspen EDR was used to design and simulate three different plate heat exchanger solutions:

- Plate heat exchangers in series where one heat exchanger utilizes the hydrogen/steam flow and the other utilizes the oxygen flow (see Figure 6).
- Plate heat exchangers in parallel where the cold stream is split between two separate plate heat exchangers in a ratio based on the thermal power available in the two hot streams (see Figure 7).

- Three-stream plate fin heat exchanger where all three streams are incorporated in one component (see Figure 8).

The intended stream sizes of this project are above but close to the lower limit of what EDR is intended for. This leads to some deviations from the actual mass flows due to the program's resolution of 0.0001 kg/s or 0.36 kg/h, which is not small enough to accurately describe the intended streams. This leads to somewhat inaccurate mass streams in the simulations. The intended mass flows and the actual values used by the program are shown in Table 5.

Table 5. The inaccuracy created by Aspen EDRs is due to a quantisation of the mass flow values within the software. This leads to small differences between actual and simulated mass flows.

Streams	Actual $\dot{m}$ [kg/h]	Simulated $\dot{m}$ [kg/h]	Inaccuracy
Oxygen	3	2.88	4.00%
Hydrogen	1.22	1.08	11.76%
Steam (total)	4.22	4.32	2.27%
Steam split oxygen:	1.25	1.08	13.36%
Steam split hydrogen	2.97	2.88	3.03%

EDR tends to suggest the same heat exchanger design for a large range of target hot stream outlet temperatures. This is likely due to operating at the extremes of the program's mass stream limits, as there are simply no smaller heat exchangers available in the library. As a result of this, the following design procedure was adopted.

An initial design was made with a very low heat recovery target, typically with the hot stream outlet set to 800˚C. This triggered the program to suggest the smallest heat exchanger it has in its library. The program suggested the same heat exchanger for temperatures down to approximately 500˚C. New designs were created by setting the target outlet temperature of the hot streams a couple of degrees centigrade lower than what the previous simulation resulted in. This triggered the program to suggest the next heat exchanger size. This process was done continuously until the hot stream outlet was close to the cold stream inlet or the cold stream outlet was close to the hot stream inlet. The simulations were conducted with 1, 5, 8 and 10 bar absolute pressure in the streams.

EDR's mass predictions for the plate heat exchangers seem to be solely based on the weight of the plates themselves, not the entire heat exchanger module. It is also only able to design plate-frame heat exchangers. This means that the mass numbers should be viewed only as an indication when investigating the trade-offs between more heat recovered and increased mass.

EDR offers a small selection of materials for the heat exchanger. Hastelloy was chosen when available. This is due to both its qualities under high temperature and for its similar weight and thermal conductivity of other high temperature resistant alloys like Inconel 625. As can be seen in Table 2 there is only a 6% density difference between Hastelloy and Inconel 625. Some initial simulations were conducted with different thermal conductivity values to investigate how changing the material would affect the outlet temperature. This led to only small differences in heat recovery even when the thermal conductivity where set drastically higher than what would

be seen when changing material. The mass of the heat exchanger does however vary more when the material is changed due to density variations between materials. This is something to keep in mind when reviewing the results of the simulations.

3.2.1 Simulations with plate heat exchangers in series

In this configuration, the two heat exchangers are used in a serial configuration. The illustration in Figure 6 shows how the first heat exchanger has a cold stream input of 200˚C steam and a hot stream of 820˚C (oxygen). The second heat exchanger uses the hydrogen hot stream at 820˚C. The cold stream is already heated from the previous oxygen heat exchangers and enters the hydrogen heat exchanger at 421˚C. The reason for this specific cold stream temperature input will be discussed in the results section.

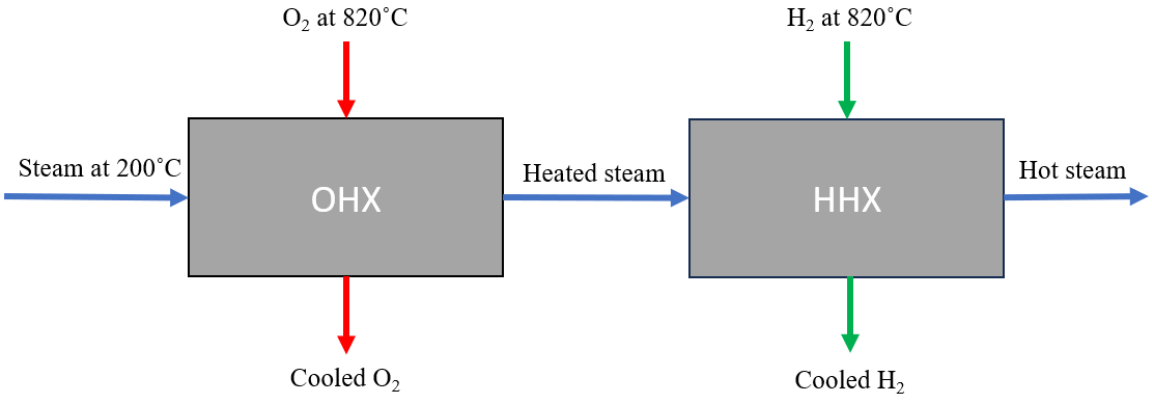

Figure 6. Configuration of serial plate heat exchangers.

The simulation was then repeated with the hydrogen stream in the first heat exchanger and the oxygen stream in the second. As can be seen in Section 4.1.2 this yielded a larger variation of designs for the first heat exchanger. As a result of this the second heat exchanger was simulated with a variety of different steam inlet temperatures based on the different simulations for the first hydrogen heat exchanger.

3.2.2 Simulations with plate heat exchangers in parallel

For a parallel plate set up the cold stream is split in two separate streams. This is done to utilise the entire temperature range in the two hot streams. The ratio of the split is determined by examining the energy in the two hot streams between 820˚C and 200˚C. This is done by using the values from Table 4Table 6 to determine a split ratio of the steam flow based on the energy in the O_2 and H_2 streams.

Table 6. To determine the split ratio of the steam to the two heat exchangers the specific enthalpy values of hydrogen and oxygen had to be evaluated.

	Hydrogen	Oxygen	Steam
$\dot{m}$ [kg/h]	1.22	3.00	4.22
$\dot{Q}$ [W]	1273	539	1560
% of total stream	0.70	0.30	
$\dot{m}$ steam in HX [kg/h]	2.97	1.25	

As can be seen in Table 6 despite having the lower mass flow the hydrogen flow contains the most thermal energy meaning that most of the steam will be sent to the hydrogen heat exchanger.

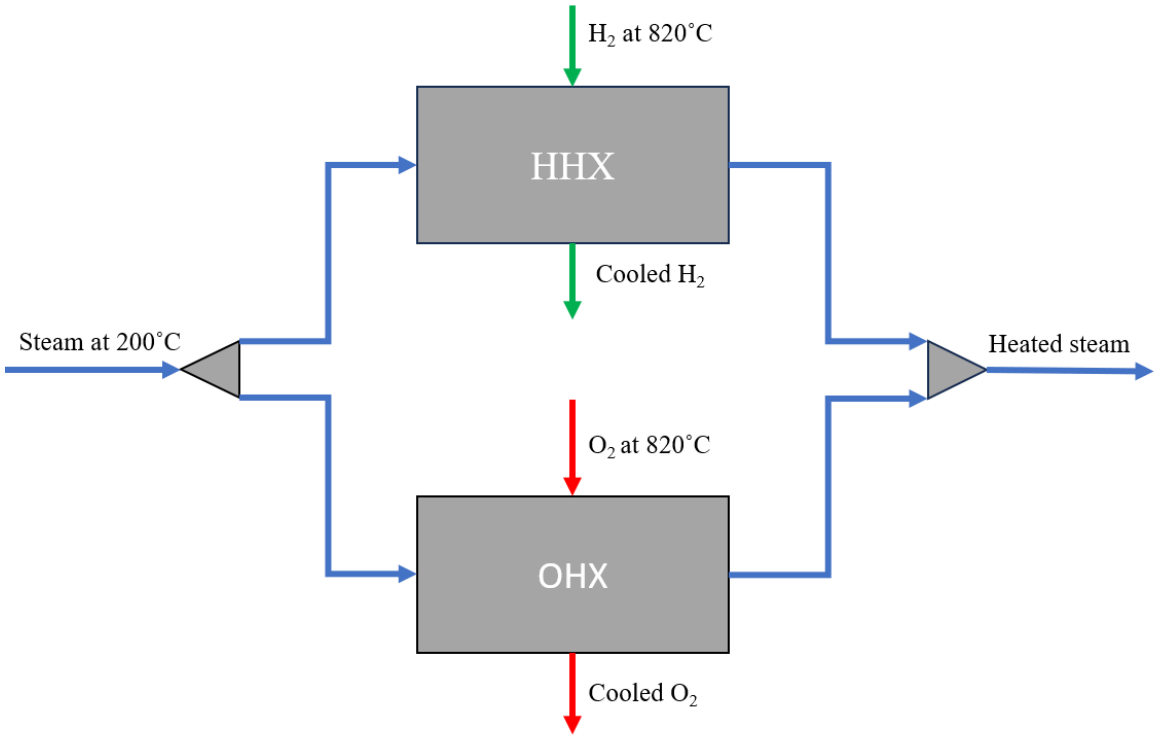

Figure 7. A schematic of the parallel heat exchanger setup.

In Figure 7 the parallel heat exchanger setup can be seen. The red arrows represent the O_2 stream, the blue is the steam flow and the green is the H_2 stream.

3.2.3 Simulations with plate fin heat exchangers

For the simulations with plate fin heat exchangers, a three-stream design is used meaning that both hot streams are used simultaneously to heat the cold stream. A flow chart can be seen in Figure 8.

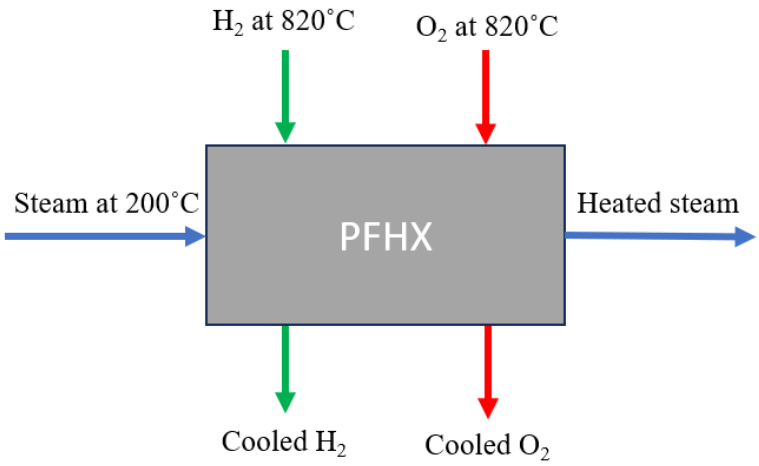

Figure 8. The schematic of a three stream plate fin heat exchanger.

It was not possible to use Hastelloy as heat exchanger material in Aspen EDR, so stainless steel was chosen as it had the closest density and thermal conductivity values to Hastelloy. Their respective heat transfer and density properties can be seen in Table 2. It is important to note that Hastelloy have approximately 15% higher density than stainless steel. This should be kept in mind when comparing the plate fin heat exchanger results to the plate heat exchanger.

3.2.4 Simulation Issues

As a result of operating on the edge of EDR's capabilities several waring messages where common when doing the simulations. The main two where related to the temperatures not being within the expected value. This indicates that the program will extrapolate values for the streams. The other warning message related to the mass flows being too small, this is already addressed in Section 3.2.

Problems also occurred when simulating the results of plate fin heat exchanger designs at higher pressures than 1 bar. This is addressed in some more detail in Section 4.3.

4. Results

In this chapter the results of the various heat exchanger simulations will be presented. The chapter is divided into subsections mimicking the format used in Chapter 3: Method.

The most important factor in choosing the best heat recovery solution is first and foremost the mass of the system compared to the amount of thermal energy it is able to recuperate. This is best visualised by examining the temperature rise of the outlet temperature in the steam. It is, after all, the main objective with the heat exchangers. To quantify this, an efficiency by means of a specific temperature change was defined where the temperature increase is seen in relation to mass.

$$\varepsilon_T = \frac{\Delta T}{m_{\mathrm{HX}}} \tag{4}$$

where ΔT is the temperature difference between cold stream outlet and input, and m_{HX} is the mass of the heat exchanger.

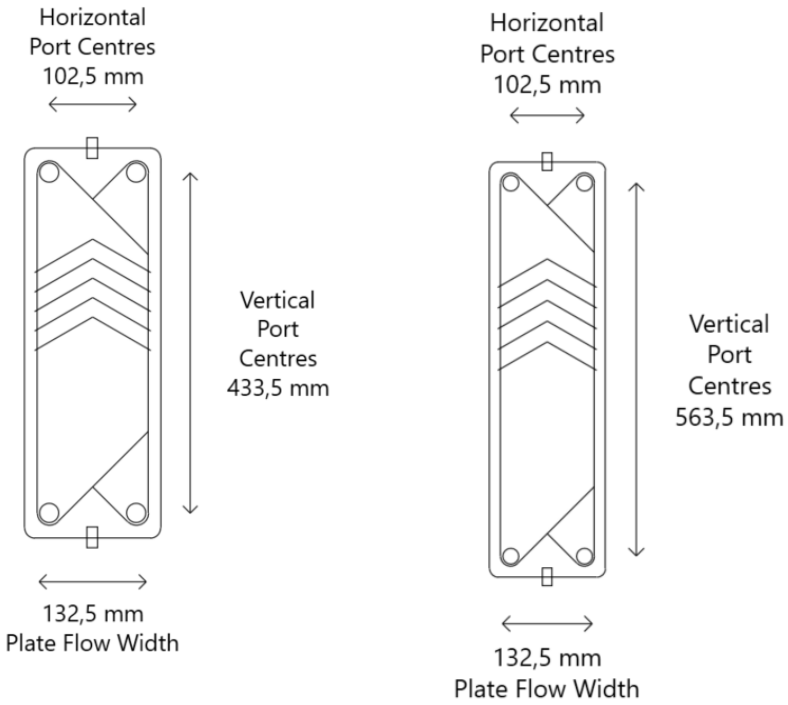

Figure 9. The figure on the left shows the smallest heat exchanger Aspen EDR designed. It is referred to as standard in the text. On the right the heat exchanger design referred to as large is displayed. It has the same dimensions as the standard design but with a slightly elongated heat transfer plate.

Two different designs were evaluated for the plate heat exchanger setups. The two designs will be referred to as standard plate and large plate, and are shown in Figure 9. The two designs are close to identical except “large” being 130 mm longer than the standard. This creates a longer path for the streams with an increase in heat transfer area, but also a correspondingly larger pressure loss. The two designs come in several configurations with between three and nine plates, and with and without two passes.

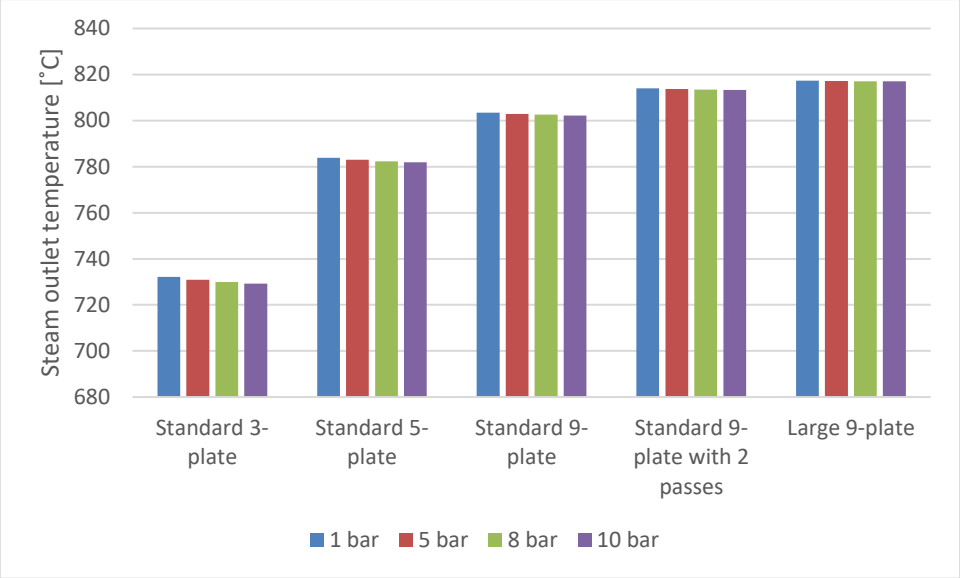

Figure 10. The mass of the heat exchangers do not change with operating pressures varying between 1 and 8 bar. A small mass increase is seen if the pressure is set to 10 bar.

Figure 10 shows that EDR estimates the same size heat exchangers for pressures up to 8 bar. When simulations were made with pressures of 10 bar there was a slight weight increase. This was due to an increase in the designed heat exchangers wall thickness from 0.6 mm up to 8 bar, to 0.7 mm for the 10 bar design.

There were also some variations in the output temperature of the heat exchangers when the operating pressure were increased. The differences were largest in the smaller heat exchangers; but they were still small, at approximately 3˚C or 0.5% difference of the temperature rise. Similar results were achieved in all the simulations for plate heat exchangers. Therefore, most of the results in the following sections will focus on simulations made with 1 bar of pressure except for in Section 4.2.1 where the results for all pressures are presented.

4.1 Plate heat exchangers in series

Two configurations of plate heat exchangers in series were simulated. Results from this simulation will be presented in these subsections. When plate heat exchangers in series are used, the steam first enters a plate heat exchanger where it receives heat from one of the two hot streams. When it leaves this heat exchanger the temperature of the steam is elevated, meaning that the second heat exchanger will not be able to utilise the temperature difference to the same degree. It is therefore important to simulate both configurations to investigate if the order of hot streams influences the total performance. A schematic representation of the heat exchangers in series can be seen in Figure 6.

4.1.1 Oxygen-hydrogen plate heat exchanger configuration

The first simulation investigates the effects of using oxygen in the first heat exchanger to heat the steam entering at 200˚C. This means that oxygen will be able to utilise most of its thermal energy available between 820˚C and 200˚C. For the heat exchanger utilising oxygen, both

standard 3-plate and standard 5-plate, were simulated yielding output temperatures of 422˚C and 428˚C. The simulation results for the standard 5-plate setup only showed an exit temperature of 201˚C for the oxygen. This indicated that the potential temperature difference of the streams was exhausted. The larger heat exchanger also only offered an increase in steam output temperature of 6˚C over the standard 3-plate setup, as can be seen in Table 7. Furter simulations with the standard 7-plate setup and onwards were therefore not conducted for the oxygen heat exchanger. It was also decided that the input value of the second heat exchanger, the chain using hydrogen, would be based on the output values of the standard 3-plate setup; giving it a steam input temperature of 422˚C.

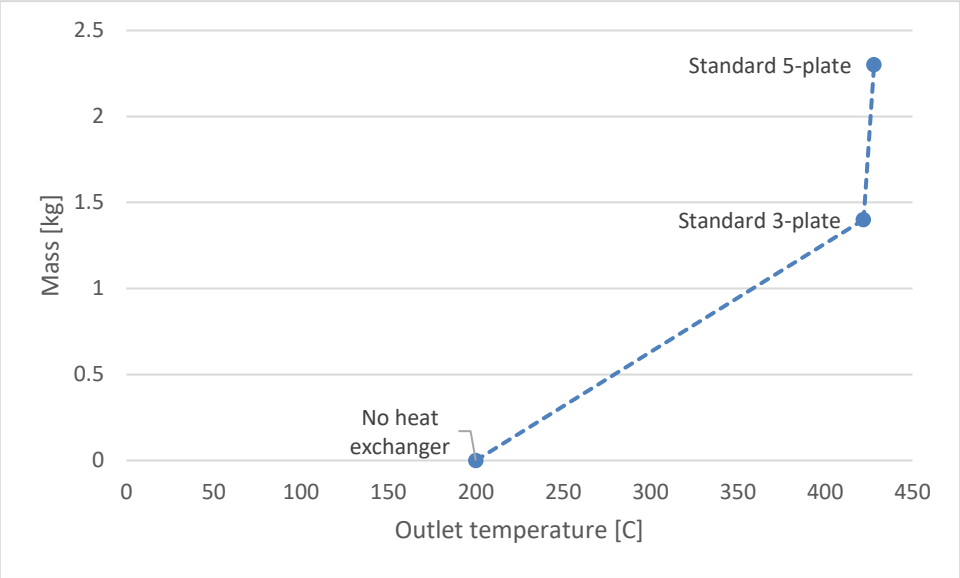

Figure 11. Results for the first heat exchanger utilising oxygen.

This is further illustrated in Figure 11 where the weight increases of adding a standard 3-plate heat exchanger comes with a large increase in outlet temperature. That said, the temperature increase for a standard 5-plate heat exchanger is barely visible when compared to the standard 3-plate heat exchanger.

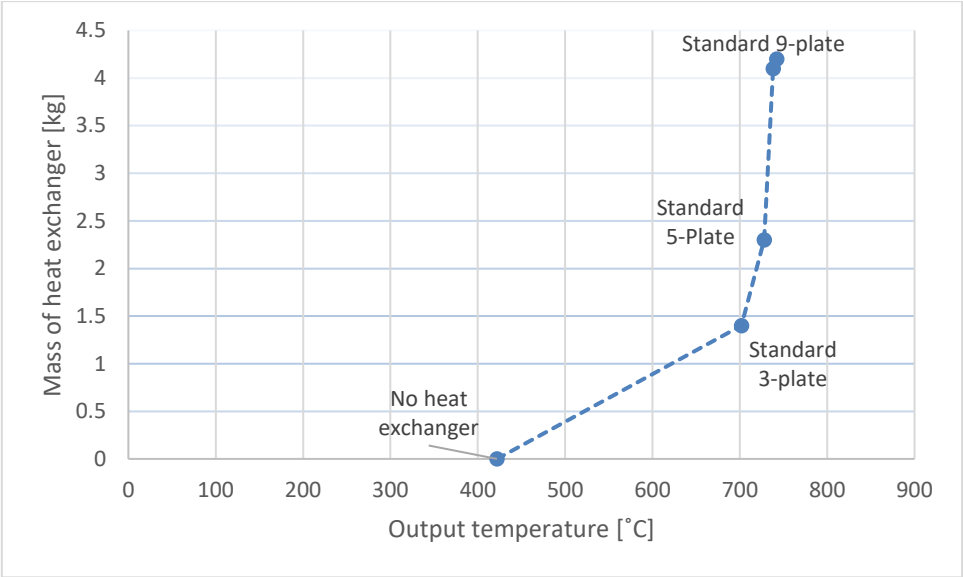

Figure 12. Results for the second heat exchanger utilising hydrogen.

Figure 12 shows how the standard 3-plate setup provides a high specific temperature change of 200 ˚C/kg. The specific temperature change decreases rapidly as the heat exchangers get larger indicating that most of the heat power has been utilised in the smaller design. It is still possible to recover more heat, but this comes at an exponential mass increase.

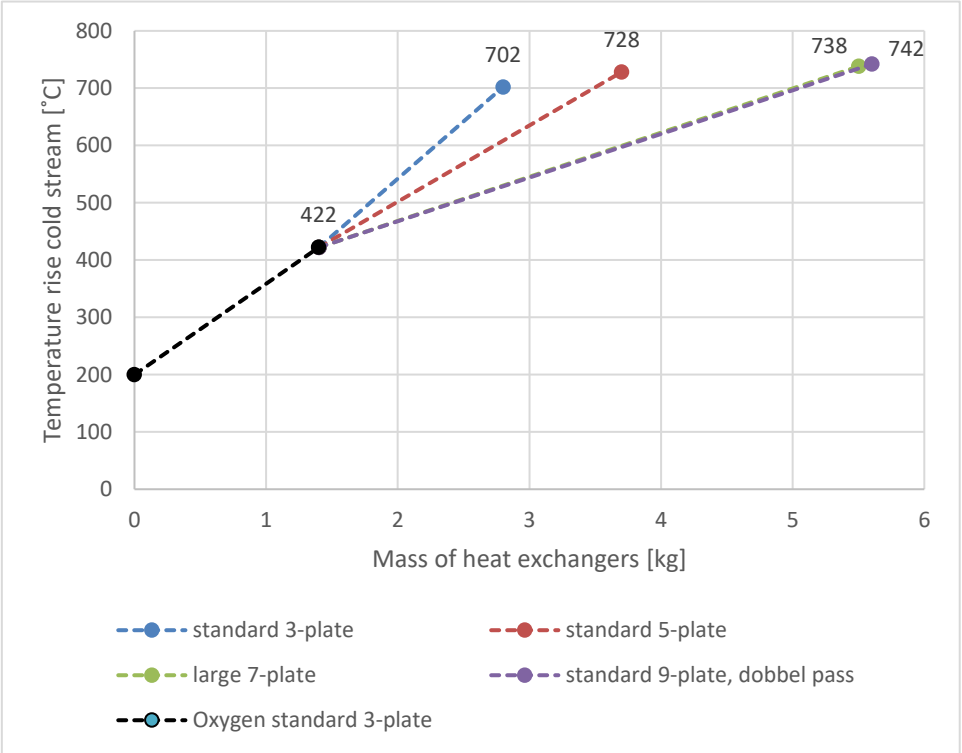

Figure 13. The combined mass for both the heat exchangers in the system and their respective outlet temperature at 1 bar of pressure.

Figure 13 shows the combined weight of the heat exchangers in the serial configuration. The temperatures on the coloured lines are the outlet temperature of the final heat exchanger. The

standard 3-plate heat exchanger is used for the first point heating the steam to 422˚C. The simulations show relatively small differences in temperature outlet when the heat exchanger gets larger, with the difference between a standard 3-plate heat exchanger and a standard 9-plate double pass heat exchanger at only 40˚C; but the mass difference is 2.8 kg. The results are also summarised in Table 7.

Table 7. The results from the simulations. HHX has a steam input temperature of 422˚C.

	Standard 3-plate	Standard 5-plate	Standard 7-plate	Standard 9-plate double pass
OHX steam outlet temperature [˚C]	422	428	-	-
Oxygen outlet temperature [˚C]	219	201	-	-
HHX steam outlet temperature [˚C]	702	728	738	742
Hydrogen outlet temperature [˚C]	476	442	428	424
Mass [kg]	1.4	2.3	3.3	4.2
System				
Outlet temperature [˚C]	702	728	738	742
Combined mass [kg]	2.8	3.7	4.7	5.6
Specific temperature change [˚C/kg]	179	143	114	97

4.1.2 Hydrogen-oxygen plate heat exchanger configuration

In this iteration of plate heat exchangers in series, hydrogen was used first. This allows for the utilisation of the hydrogen's thermal energy between 820˚C and 200˚C. This yielded more variations for the first heat exchanger compared to when oxygen was used first. For this reason, both 3, 5, 7 and 9-plate standard heat exchangers were simulated for the hydrogen stream. For the second heat exchanger using oxygen as the hot stream, both a standard 3-plate and a standard 5-plate setup were simulated. It was discovered that using the larger heat exchanger only produced a 1˚C difference in outlet temperature. As a result of the small difference in temperature just the standard 3-plate heat exchanger was investigated further. Figure 14 shows the outlet temperature of different heat exchangers for the hydrogen stream coupled with a standard 3-plate heat exchangers. New simulations for the second heat exchanger were done to match each of the different outlet temperatures of the designs. The mass shown is the combined mass of the heat exchangers in the respective setups.

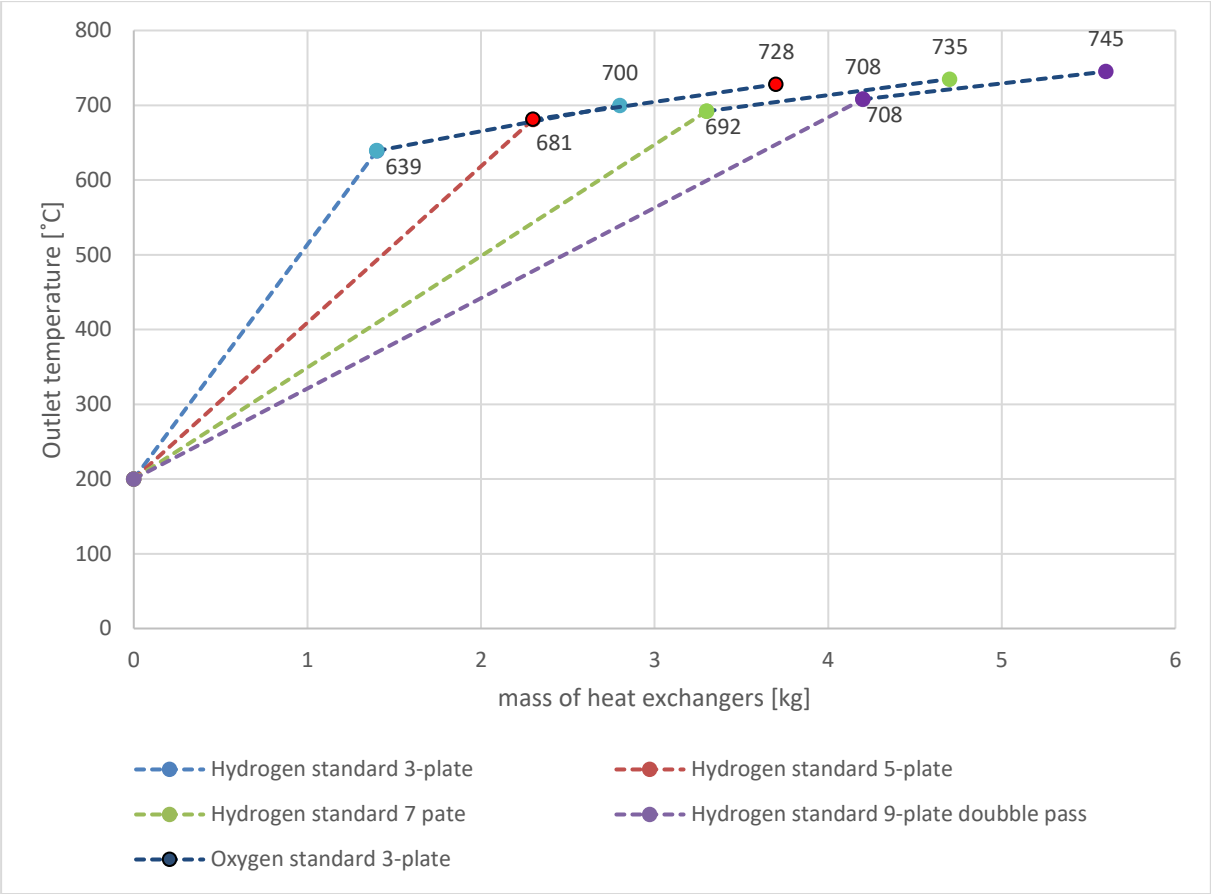

Figure 14. Results for the combined system of different heat exchangers for the hydrogen and a standard 3 plate heat exchanger for the oxygen.

In Table 8 the mass of both the heat exchangers is shown together with the resulting outlet temperature of the streams. Note that when using the standard 9-plate double pass heat exchanger for the hydrogen stream, the outlet temperature of the hydrogen is 209˚C indicating that most of the recoverable heat is used. This does however lead to a high inlet temperature for the following oxygen-based heat exchanger making it almost obsolete. In this configuration the second heat exchanger is only able to utilise a temperature difference of 90˚C.

Table 8. Combined results for the heat exchangers in series under 1 bar of operating pressure.

	Standard 3-plate	Standard 5-plate	Standard 7-plate	Standard 9-plate double pass
Steam outlet temperature [˚C]	700	728	735	745
Hydrogen outlet temperature [˚C]	300	244	229	209
Oxygen outlet temperature [˚C]	642	683	694	710
Mass [kg]	2.8	3.7	4.7	5.6
Specific temperature change [˚C/kg]	179	143	114	97

Additional data from the simulation can be found in attachment 1a.

4.2 Plate heat exchanger in parallel

The results from the simulations of heat exchangers in parallel is presented in two subsections, one for each of the heat exchangers.

4.2.1 Results for the hydrogen heat exchanger

Five different designs were investigated for the hydrogen heat exchanger. Simulations were also performed for higher pressures up to 10 bar.

Figure 15 shows how increasing the pressure has a small influence on the heat exchanger outlet temperature, predominantly in the smaller heat exchangers. In the standard 3-plate setup a difference of 2.99˚C can be observed between the 1 bar and 10 bar streams. This temperature difference has fallen to 0.35˚C in the large 9-plate setup.

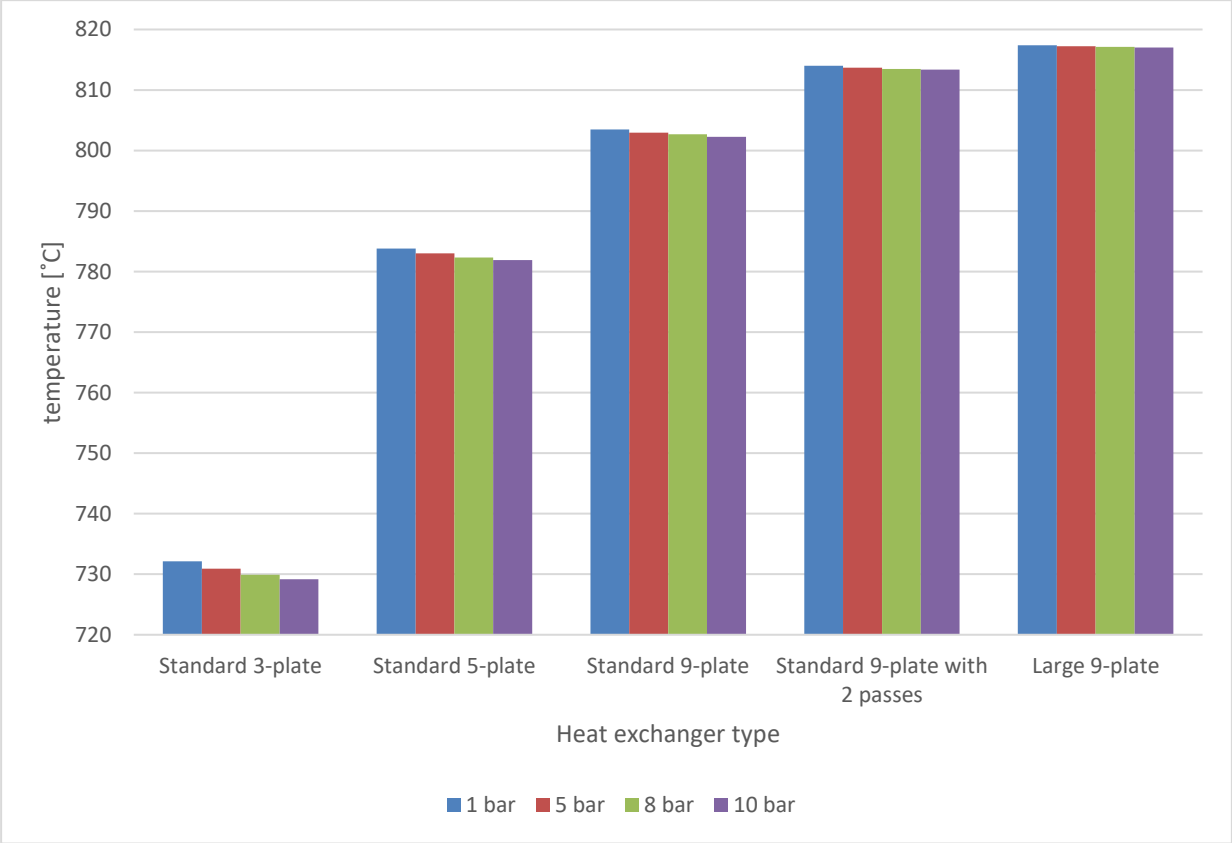

Figure 15. Change of outlet temperature in different heat exchangers when pressure is increased.

In Table 9 the data from Figure 15 is shown. There are only small changes in outlet temperature observable in the smaller heat exchangers. For the large 9-plate heat exchanger, no change is seen when the operating pressures are increased.

Table 9. Outlet temperatures of the various heat exchangers with operating pressures between 1 and 10 bar.

	Standard 3-plate	Standard 5-plate	Standard 9-plate	Standard 9-plate double pass	Large 9-plate
Outlet temperature at 1 bar [˚C]	732	784	804	814	817
Outlet temperature at 5 bar [˚C]	731	783	803	814	817
Outlet temperature at 8 bar [˚C]	730	782	803	813	817
Outlet temperature at 10 bar [˚C]	729	782	802	813	817

Figure 16 shows how the mass of the heat exchanger drastically increases when the outlet temperature of the steam approaches the inlet temperature of the hydrogen. The lateral jump in temperature recovered at 4 kg is due to the use of two passes within the same heat exchanger. This increases the outlet temperature by 10˚C without adding any weight to the unit.

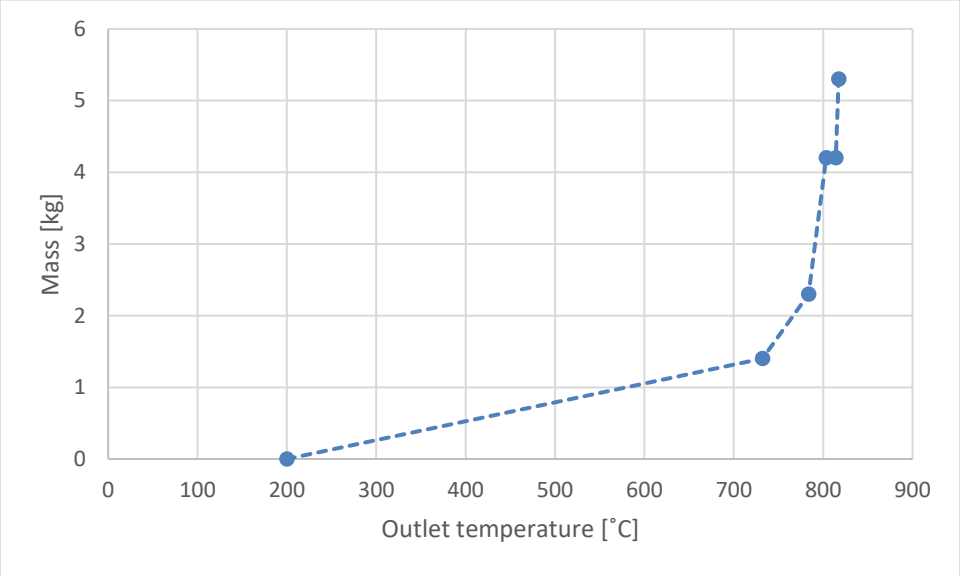

Figure 16. The relation between the outlet temperature of the heat exchanger and how the weight increases as the size get bigger. The simulations are done with 1 bar of operating pressure.

Table 10 shows results for the simulations. Note the different outlet temperature of standard 9-plate and standard 9-plate with two passes. These two configurations are the same size and mass but differ in their internal path. This leads to the two-pass configuration yielding an outlet temperature that is 10˚C higher than the one-pass design.

Table 10. Results from hydrogen split stream heat exchanger with an operating pressure of 1 bar.

	Standard 3-plate	Standard 5-plate	Standard 9-plate	Standard 9-plate with 2 passes	Large 9-plate
Cold stream outlet [˚C]	732	784	804	814	817
Hot stream outlet [˚C]	387	340	321	312	308
Mass [kg]	1.4	2.3	4.2	4.2	5.3
Specific temperature change [˚C/kg]	380	254	144	146	116

4.2.2 Results for the oxygen-fed heat exchanger

Simulations for the oxygen-fed heat exchanger result in steam outlet temperatures very close to the results from the hydrogen-fed heat exchanger. This indicates that the calculations for the split ratio of the steam are correct. The small inaccuracies that are found are assumed to be rounding errors.

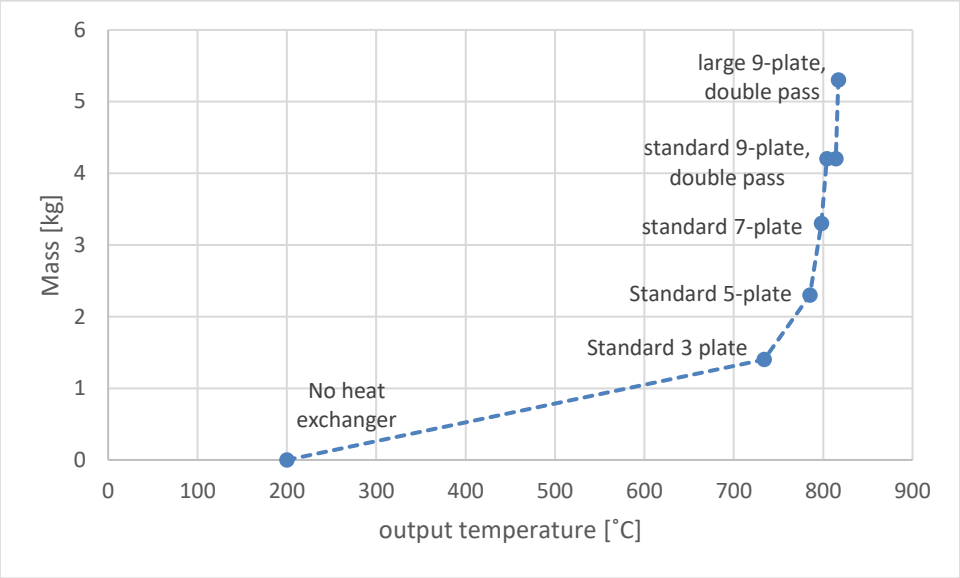

Figure 17. Results for oxygen-fed heat exchanges at 1 bar. Higher outlet temperatures are possible with a larger heat exchanger. The size and mass of the heat exchanger do however not scale linearly in relation to outlet temperature.

Figure 17 shows how an increasingly large heat exchanger is needed when the cold stream approaches the hot stream inlet temperature. It is possible to get the outlet temperature very close to the hot stream inlet temperature, but this comes at a considerable mass penalty.

Table 11. Results of the parallel heat exchanger using oxygen as hot stream.

	Standard 3-plate	Standard 5-plate	Standard 9-plate	Standard 9-plate with 2 passes	Large 9-plate
Cold stream outlet [˚C]	734	785	804	814	817
Hot stream outlet [˚C]	387	330	311	302	298
Weight [kg]	1.4	2.3	4.2	4.2	5.3
Specific temperature change [˚C/kg]	380	254	144	146	116

In Table 11 the results from the oxygen-fed parallel heat exchanger simulations are presented. Note that the hot stream outlet temperature is 298˚C when oxygen exits the heat exchanger. This indicates that it is the outlet temperature of the steam approaching the inlet temperature of the oxygen that is the limiting factor and not a need for more heat power.

Additional data from the simulation can be found in attachment 1b.

4.3 Results for the plate fin heat exchanger

The results of the simulations of a three-stream plate fin heat exchanger at 1 bar of pressure can be seen in Figure 18. The graph shows an almost linear increase of mass up to 770˚C, but past this the weight increases drastically.

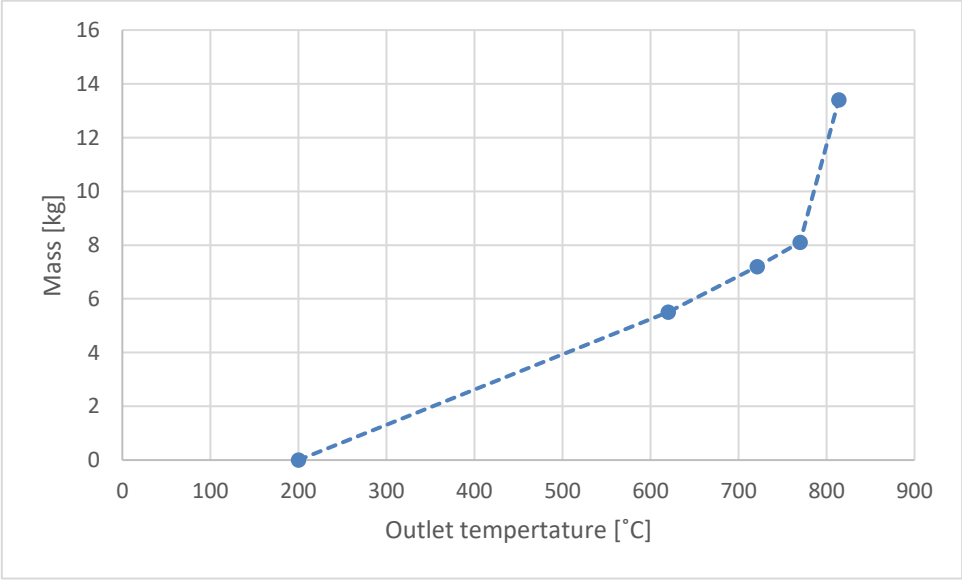

Figure 18. Relation between mass and outlet temperature of a three-stream plate fin heat exchanger under 1 bar of pressure.

When the pressure was increased, the program would still design new heat exchangers. However, when switched into simulation mode it would refuse to run the simulation unless some parameters were changed manually. As this would deviate from the other simulations that

were carried out where the suggested heat exchanger design is used without user interference, this was not done.

Table 12. Estimates from the design and the results from the simulation with 1 bar of operating pressure.

Design inlet temperature [˚C]	500	400	350	300
Design results				
Steam outlet temperature [˚C]	595	706	759	812
Mass [kg]	5.7	7.2	8.1	13.4
Simulation results				
Steam outlet temperature [˚C]	620	721	770	814
Mass [kg]	5.5	7.2	8.1	13.4
Specific temperature change [˚C/kg]	76.4	100	95.1	60.8

Table 12 is divided into two sections. The result of the design process is presented first. This is the heat exchanger EDR suggests as a solution to reach the target outlet temperatures of the hot streams (design inlet temperature) chosen. It also gives an estimate of what the outlet temperature of steam will be with the suggested solution, but with a safety factor built in. Then the simulation results are shown. They are the result of what the program estimates will be the actual value for the chosen heat exchanger. All of the simulations and designs presented in Table 12 are done at 1 bar of operating pressure. The results show a 25˚C temperature difference in the smallest heat exchanger design when compared to the simulation result. The deviation between estimated and the simulated outlet temperature decreases as the size of the heat exchanger grows.

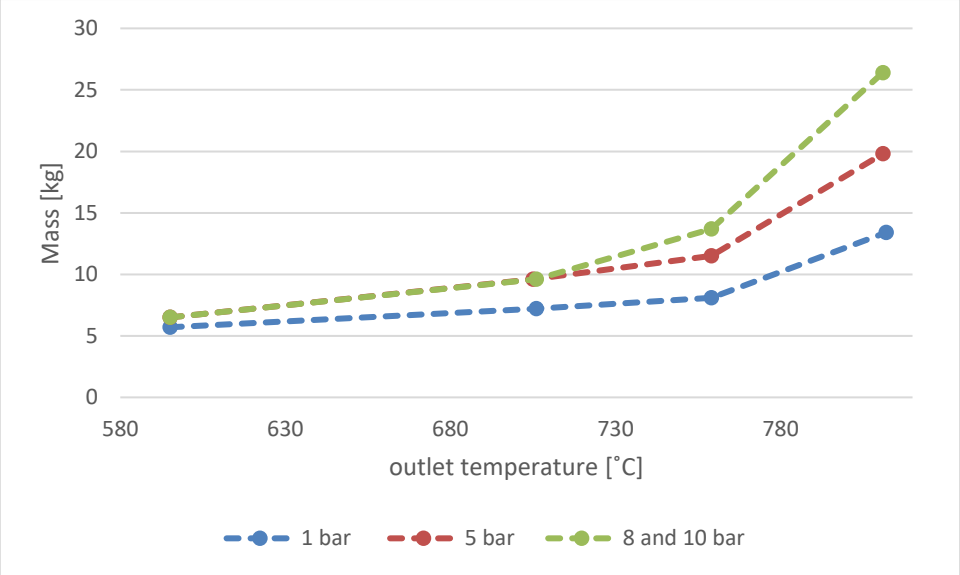

Figure 19 Design masses and outlet temperatures for the high-pressure designs.

Figure 19 is based on the design estimates and not the simulation results. The 1 bar line is made with the same design inlet temperatures that were used for the simulation in Figure 18.

The graphs in Figure 19 show the same trend for 1 bar of pressure as seen in Figure 18, with a close to linear relationship between increasing outlet temperature and mass. This continues until the largest heat exchanger, where the mass increases more rapidly. For pressures of 8 and 10 bar the mass to outlet temperature relation is not linear; it gradually increases as the outlet temperature increases. The 8 and 10 bar designs have the same mass through all the outlet temperatures, whilst 5 bar design correlates for the two smaller temperatures; but not the two largest. Increasing the operating pressure has a large impact on the mass of the plate fin design. The largest difference of mass between the heat exchangers is 13 kg for the same outlet temperature with different operating pressures.

Additional data from the simulations can be found in the Attachments 1c.

5. Discussion

This chapter will discuss both the results from the simulations as well as findings during the literature search. It is divided into sections based on the findings, followed by a short discussion on what the reasons and implications of this might entail.

5.1 Plate heat exchanger

The simulations for the two different plate heat exchanger configurations, parallel and serial, yielded fairly similar results. When using the 1.4 kg standard 3-plate heat exchanger for all the parts of the system, the difference in outlet temperature between the serial and parallel configuration was only 30˚C. When deciding what solution is the best, other parameters might be more important than the extra 30˚C of elevated steam temperature which could be achieved with the parallel configuration such as mass increase. If a parallel configuration is chosen, a unit to split the flow of steam needs to be implemented upstream. Likewise, a mixing chamber for the steam downstream has to be integrated into the setup. This solution, in combination with the extra pipes needed when there are two flows of steam, could end up adding significant additional mass to the system, which could outweigh the benefit of the 30˚C temperature increase of the steam. It could be more mass efficient to have a larger heat exchanger in a serial configuration. A setup with parallel heat exchangers could however have other advantages. Depending on the robustness of the stream splitter and given that both the heat exchangers have a large enough capacity to handle the whole steam flow, the parallel configuration offers more reliability with the possibility to route all the steam to one of the heat exchangers in case either one or the other breaks down.

The serial configurations of heat exchangers did not provide the highest steam outlet temperatures; they do however possess some valuable possibilities. The outlet temperature of both H_2 first or O_2 first are so similar that it is possible to target which hot stream to cool down. This way the outlet temperature of the hot stream can achieve considerably lower temperature than the alternatives compared to the size of the heat exchanger. In the same way, the stream that is not cooled has a higher outlet temperature than any other configuration. This heat might be utilised in an ISRU operation of heat demanding equipment.

The parallel heat exchanger configuration provided the highest outlet temperature of the simulations. Small differences in the outlet temperature were observed between the heat exchangers. When the heat exchangers were designed, the streams were split based on specific enthalpy values in an effort to gain the same temperature increase in both heat exchangers. When reviewing the results, a possible error source was discovered. When deciding the split ratio between the heat exchangers, the mass flow used for the steam was not corrected for EDR's limitations in small mass flows. This caused EDR to direct more steam to the H_2 heat exchanger than intended, based on the calculation results shown in Table 6. Due to time constraints, new simulations with altered values to compensate for this were not conducted.

The results from the simulations using the actual split ratio can still provide important insight. Sending more steam to the H_2 heat exchanger should in theory lower the outlet temperature

rather than increase it. It is therefore assumed that the elevated temperature of the H_2 heat exchanger is a result of rounding errors and the considerably higher heat transfer coefficient of H_2 compared with O_2. The largest difference occurs in the smaller heat exchangers when a 2˚C difference can be seen in the outlet temperature of steam. The outlet temperature for the hot streams is identical in this case. This indicates that the amount of heat is the limiting factor, as the temperature interval that is experienced by the hot streams are also identical. When the heat exchanger is of a larger design, the difference in outlet temperature of steam decreases. The outlet temperature of the O_2 does however become lower than that of the H_2. The reason for this might be that the larger heat exchanger is able to utilise a larger temperature difference to compensate for the lower amount of available heat in the O_2 stream. At the same time, the temperature of the H_2 stream is approaching that of the inlet hot stream, so that the benefit of a larger heat exchanger is minimal.

Electric heaters are effective at converting electricity to thermal energy with a coefficient of performance (COP) close to 1. As an electric heater would have to be included in the system to ensure that the steam reaches the operating temperature, it is relevant to investigate the actual power savings of the heat exchanger setup. The same method that was used in 3.1 to decide the amount of thermal power in the streams can be used to calculate the amount of recuperated power.

Table 13. Summary of estimated power savings.

	Recovered thermal power [kW]	Electric heater power demand [kW]	Power reduction [%]	Mass [kg]	PV mass [kg]	Total mass [kg]
No heat exchanger	0	1.56	0	0	9.2	9.2
Serial double standard 3-plate	1.24	0.32	79.5	2.8	1.9	4.7
Parallel double standard 3-plate	1.33	0.23	85.3	2.8	1.4	4.2
Serial 3 + 9 standard plate	1.34	0.22	83.6	5.6	1.3	6.9
Parallel double standard 9-plate	1.55	0.01	99.4	8.4	0.1	8.5

Table 13 shows that 1.24 kW of thermal power was recuperated in serial configuration with the standard 3-plate heat exchanger for both hot streams. When a 9-plate heat exchanger was used for the H_2 stream, only 0.1 kW more was recovered at a mass increase of 2.8 kg. For the parallel heat exchanger configuration 1.33 kW was recuperated with standard 3-plate and 1.55 kW with 9-plate heat exchangers. The extra 0.22 kW came at a mass penalty of 5.6 kg. The PV mass shows the estimated mass of solar cells needed to generate the remaining electric power demand. The total mass shows the combined system of PV solar cells and heat exchangers. Based on the results, all the combinations of heat exchangers yield mass savings. The parallel double standard 3-plate solution offers the best solution by mass.

5.2 Plate fin heat exchanger

The Plate Fin Heat Exchanger (PFHE) simulations encountered several problems, which were discussed in Section 4.3. This included problems with the software not being able to run the simulation at elevated pressures. This makes the results somewhat inconclusive, and more research should be conducted before this design is eliminated. Some knowledge can however still be gained from the results. The mass of the three-stream plate fin heat exchanger is considerably heavier than an equivalent solution with two plate heat exchangers. This could be a result of inaccuracies in the program, or it might be a result of the construction of the plate fin heat exchanger. The benefit of this design is the extra heat transfer surface per volume created by the fins. This typically makes them smaller in size compared to other heat exchanger designs with more heat transfer area per unit volume; however, this is also a disadvantage as the added fins add more mass to the heat exchanger. For the specific case of space applications, mass savings are critical. This means that the added heat transfer surface the fins provide might not justify the added mass. There is also a possibility that the results for plate fin heat exchangers include the mass of the entire module. This would make a direct comparison with the plate heat exchanger results, which only measure the mass of the plates, unfair. That said, it does give an indication of thermal energy recovered and an estimate of size.

As a result of the problems encountered when simulating with high operating pressures, only the design function in EDR was used. Based on results obtained with the design function, plate fin heat exchangers were more susceptible to pressure increases in comparison with regular plate heat exchangers in relation the mass increase. A possible explanation might be that the EDR library does not contain plate fin heat exchanger designs for high operating temperatures. This can also explain the limited choices in material given, as aluminium would not be suitable for this application due to the high temperatures. The poor results achieved by the plate fin heat exchanger in general are somewhat surprising as this is the typically suggested solution for gas-to-gas applications according to literature [34], [35].

5.3 Other findings

The system should be scalable because the hot and cold streams are all coming from the same source. If the O_2 production is increased, more steam would need to be heated. As the heat source for the steam is the H_2 and O_2 it will all scale at the same rate. However, no simulations were performed to confirm this hypothesis.

Cooling gases to cryogenic temperatures is usually a very energy demanding process. The specific energy need to cool H_2 and O_2 from 820˚C to their respective liquid state is 2.4 kW for the H_2 and 0.8 kW for the O_2 [42]. Note that the actual energy demand for liquification is much larger. Large scale H_2 liquefying plants on Earth typically have an energy consumption of more than 10 kWh/kg_{LH2} [45]. If this cooling process could be combined with the extracting process of the water ice, large energy savings would be possible. As a result of the extremely low temperature of the Permanently Shadowed Regions (PSRs) the water ice targeted for ISRU will hold the same low temperature. This might make it possible to utilise the waste heat from the SOE further. If the streams of O_2 and H_2 could be routed in a way to melt the ice it would both save energy in the extraction process of water, and also the liquification of O_2 and H_2.

The choice of power supply for a lunar base will impact the choice of solution for heat recuperation. Depending on design, nuclear power may deliver a power to mass ratio as low as 6.5 W/kg. In this case the 220 W of recuperated thermal power at a mass penalty of 5.6 kg might be an attractive alternative. On the other hand, the nuclear reactors in development for the Moon will use Stirling engines to produce electricity. This would mean that the operating temperature might be higher than what is normally seen in steam turbines on Earth. This could provide better sources for waste heat recouperation than the exhaust gases of the SOE. It then comes down to a matter of efficiently cooling the H_2 and O_2, rather than energy savings.

Using a heat exchanger instead of electric heating also cools down the hot oxygen and hydrogen streams. This needs to be done anyway before both gases can be stored. It is also important to keep in mind that there are unseen mass savings due to a less complicated cooling setup with fewer parts when heat exchangers are utilised.

For a final design of the thermal system, the inlet temperature of the heat exchangers could be set to the outlet temperature of the boiler. This would eliminate the need for an additional electric heater to superheat the steam between the boiler and heat exchanger. This will also enable the heat exchanger to utilise waste heat from an even larger temperature range.

When EDR is used for designing the heat exchangers, the smallest alternative provides the best outlet temperature to mass ratio. This might indicate that because of operating on the edge of EDR's intended stream sizes, the program is constrained by its available library of heat exchanger designs. This might mean that an even smaller heat exchanger would be the ideal design, with an improved balance between heat recouped and added mass to the system achievable.

A decrease in steam outlet temperature was observed when the pressure was increased in the heat exchangers. This is likely due to the increased density in the gases leading to lower speeds through the exchanger. This in turn leads to less turbulence and mixing in the stream. At the same time the decrease in outlet temperature is somewhat counter intuitive as the residency time inside the heat exchanger is increased. There are only negligible differences in the steam's viscosity between 1 and 10 bar at these temperatures. The H_2 has a 16% increase and O_2 has a 34% increase in viscosity. The increase in viscosity could be helping to counter some of the lost turbulence and explain why the temperature drop is relatively low.

The simulation shows that increasing the pressure in the plate heat exchanger has a very small effect on the outlet temperature. There are no significant changes until the pressure reached 10 bar. At 10 bar the heat exchanger weight increased due to an increase of 0.1 mm to the plates thickness. Even though it is not shown in the simulation results, increasing the pressure will likely have more implications. Under high pressure gasket-based plate heat exchangers can start to leak. Plate heat exchangers used under high pressure are therefore typically braced instead. This makes them more difficult to service. Even though the plate heat exchangers scaled well with elevated pressures, during the simulation there will likely be other system wide implications. All tubing, caskets, containers and so on would also need to be pressure resistant. This will likely lead to much larger mass increases than seen in the heat exchangers.

The water ice found at the Moon contains several volatiles as seen in Table 1. This means fouling might pose a risk for the heat exchanger. Due to the simulation only using pure steam, O_2 and H_2 no results for fouling were gained. Even though solid oxide electrolysis has a high tolerance to impurities in the steam some kind of cleaning process will likely be implemented in the ISRU process. Simulations investigating fouling issues should be revisited at a later stage when more data for the steam composition is available.

With the development of additive manufacturing, new and more advanced geometries in the heat exchanger design are possible. These relatively new designs may make smaller, lighter and more efficient heat exchangers possible [46]. As the results from the simulations show there is enough thermal energy in the hot streams to raise the temperature in the steam very close to 820˚C. The limiting factor is however the mass of the heat exchanger needed to reach this temperature. The potential mass savings additive manufacturing offers might be a solution to this.

6. Conclusion

The conclusion is divided in two sections. A summary of the main conclusions that can be drawn based on the research conducted and suggestions for further work.

6.1 Conclusion

The result of this project indicates that using a heat exchanger to recover thermal energy from the SOE products to heat up the SOE inputs is beneficial. Different heat exchanger designs where investigated. Both a parallel and serial heat exchanger configuration yield similar results with respect to recovered heat and mass of the heat exchangers. The serial heat exchanger setup achieved 1.24 kW recovered thermal power while parallel achieved 1.33 kW at a mass of 2.8 kg. The highest recovery achieved was with a parallel heat exchanger using two 9-plate heat exchangers. This configuration recovered 1.55 kW at a mass of 8.4 kg. This means that the initial power needed to heat the steam with an electric heater, 1.56 kW can be reduced with between ~ 80 to 99% depending on the size of the heat exchanger. All the solutions including heat exchangers represent a significant lowering in total mass compared to using PV solar cells to generate the necessary electricity for heating the steam.

Parallel configuration achieves the largest temperature increase compared to mass of the heat exchangers. This solution will however need more infrastructure up- and downstream in the form of a splitter and a mixing chamber. This might end up making this a more mass intensive choice.

It is hard to conclude what the most suitable solution is with such a broad mission plan. Both versions of plate heat exchangers have their advantages. Depending on the mission, there might be several possible synergy effects that will dictate which solution is more attractive. If it is beneficial to cool one of the hot streams as much as possible, serial heat exchangers will be the best choice.

Small differences in outlet temperature were observed when the operating pressure of the heat exchangers was increased. The same plate heat exchanger could be used up to 8 bar. At 10 bar, the mass increased because of thicker plates being necessary to withstand the pressure forces. Plate fin heat exchangers did not scale well with increased pressure as the mass increased drastically.

6.2 Further work

Plate fin heat exchangers could not be investigated as thoroughly as the other heat exchangers due to limitations in the software. As this is the most common heat exchanger for gas-to-gas applications, this solution should be investigated further with better suited tools before dismissing it.

The software used for the simulations is not designed to simulate very small mass flows and high temperatures. This leads EDR to suggest the same heat exchanger size for several target temperatures. There might be a better balance between heat recuperation and mass beyond

EDR’s capabilities. This means that the results might be misleading and further investigations with more suitable software and practical tests for verification should be conducted. ANSYS could be used to design a custom heat exchanger and also provides the possibility to take advantage of the possibilities created by the advancements in additive manufacturing. Recent advancements in 3D printing make it possible to design more exotic heat exchangers utilising advanced geometries. This might provide more efficient solutions than provided by EDR and warrants an investigation.

References

[1] ‘Annual number of objects launched into space’, Our World in Data. Accessed: Dec. 09, 2023. [Online]. Available: https://ourworldindata.org/grapher/yearly-number-of-objects-launched-into-outer-space

[2] NASA, ‘NASA’s Lunar Exploration Program Overview’. Sep. 2020. Accessed: Dec. 09, 2023. [Online]. Available: https://www.nasa.gov/wp-content/uploads/2020/12/artemis_plan-20200921.pdf

[3] ‘Mars is Closer Than You Think – Red Planet Dispatch’. Accessed: Dec. 09, 2023. [Online]. Available: https://blogs.nasa.gov/redplanetdispatch/2018/03/06/mars-is-closer-than-you-think/

[4] Y. Akisheva and Y. Gourinat, ‘Utilisation of Moon Regolith for Radiation Protection and Thermal Insulation in Permanent Lunar Habitats’, *Appl. Sci.*, vol. 11, no. 9, Art. no. 9, Jan. 2021, doi: 10.3390/app11093853.

[5] M. Isachenkov *et al.*, ‘Technical evaluation of additive manufacturing technologies for in-situ fabrication with lunar regolith’, *Adv. Space Res.*, vol. 71, no. 6, pp. 2656–2668, Mar. 2023, doi: 10.1016/j.asr.2022.07.075.

[6] ‘Your Guide to Water on the Moon’, The Planetary Society. Accessed: Oct. 03, 2023. [Online]. Available: https://www.planetary.org/articles/water-on-the-moon-guide

[7] E. Detsis, O. Doule, and A. Ebrahimi, ‘Location selection and layout for LB10, a lunar base at the Lunar North Pole with a liquid mirror observatory’, *Acta Astronaut.*, vol. 85, pp. 61–72, Apr. 2013, doi: 10.1016/j.actaastro.2012.12.004.

[8] ‘NASA Moon Camera Mosaic Sheds Light on Lunar South Pole - NASA’. Accessed: Oct. 09, 2023. [Online]. Available: https://www.nasa.gov/missions/lro/nasa-moon-camera-mosaic-sheds-light-on-lunar-south-pole/

[9] T. M. Pelech, G. Roesler, and S. Saydam, ‘Technical evaluation of Off-Earth ice mining scenarios through an opportunity cost approach’, *Acta Astronaut.*, vol. 162, pp. 388–404, Sep. 2019, doi: 10.1016/j.actaastro.2019.06.030.

[10] H. Song *et al.*, ‘Investigation on in-situ water ice recovery considering energy efficiency at the lunar south pole’, *Appl. Energy*, vol. 298, p. 117136, Sep. 2021, doi: 10.1016/j.apenergy.2021.117136.

[11] X. Li, *Principles of fuel cells*, 1st ed. New York: Taylor & Francis Group, LLC, 2005. [Online]. Available: https://doi.org/10.1201/9780203942338

[12] A. Colaprete *et al.*, ‘Detection of water in the LCROSS ejecta plume’, *Science*, vol. 330, pp. 463–8, Oct. 2010, doi: 10.1126/science.1186986.

[13] J. A. Hoffman, E. R. Hinterman, M. H. Hecht, D. Rapp, and J. J. Hartvigsen, ‘18 Months of MOXIE (Mars oxygen ISRU experiment) operations on the surface of Mars - Preparing for human Mars exploration’, *Acta Astronaut.*, vol. 210, pp. 547–553, 2023, doi: https://doi.org/10.1016/j.actaastro.2023.04.045.

[14] G. Omdal, ‘Clara (previously Prototech) and CERTH awarded contract for production of fuel and oxygen from lunar and Martian resources’, Clara. Accessed: Oct. 03, 2023. [Online]. Available: https://claraventurelabs.com/news/clara-previously-prototech-and-certh-awarded-contract-for-production-of-fuel-and-oxygen-from-lunar-and-martian-resources

[15] S. Noble, ‘The Lunar Regolith’, presented at the Lunor Regolith Simulant Workshop, Alabama, Mar. 2009. Accessed: Nov. 21, 2023. [Online]. Available: https://ntrs.nasa.gov/citations/20090026015

[16] T. Stubbs, R. Vondrak, and W. Farrell, ‘Impact of Dust on Lunar Exploration’, *Dust Planet. Syst.*, pp. 239–243, Jan. 2007.

[17] H. Noda *et al.*, ‘Illumination conditions at the lunar polar regions by KAGUYA(SELENE) laser altimeter’, *Geophys. Res. Lett.*, vol. 35, no. 24, 2008, doi: 10.1029/2008GL035692.

[18] ‘Moon Fact Sheet’. Accessed: Dec. 03, 2023. [Online]. Available: https://nssdc.gsfc.nasa.gov/planetary/factsheet/moonfact.html

[19] M. Haese, Pat George, Takeshi Hoshino, Lee Mason, and R. Gabe Merrill, ‘A power architecture for the ISECG reference architecture for human lunar exploration’, *61st Int. Astronaut. Congr. Prague CZ.*

[20] M. Kaczmarzyk and M. Musiał, ‘Parametric Study of a Lunar Base Power Systems’, *Energies*, vol. 14, no. 4, Art. no. 4, Jan. 2021, doi: 10.3390/en14041141.
[21] Ivar Wærnhus, ‘European Charging Station for the Moon (ECSM) -Ongoing project by Space Applications Services, Clara Venture Labs mm.’, Dec. 18, 2023.
[22] C. Chen, H. Mei, M. He, and T. Li, ‘Neutronics analysis of a 200 kWe space nuclear reactor with an integrated honeycomb core design’, *Nucl. Eng. Technol.*, vol. 54, no. 12, pp. 4743–4750, Dec. 2022, doi: 10.1016/j.net.2022.08.012.
[23] ‘UK Space Agency funds Rolls-Royce to develop Moon base nuclear power - Nuclear Engineering International’. Accessed: Dec. 14, 2023. [Online]. Available: https://www.neimagazine.com/news/newsuk-space-agency-funds-rolls-royce-to-develop-moon-base-nuclear-power-10694239
[24] H. W. Jones, ‘The Recent Large Reduction in Space Launch Cost’, in *2018-07-08*, Albuquerque, NM. Accessed: Nov. 22, 2023. [Online]. Available: https://ntrs.nasa.gov/citations/20200001093
[25] ‘Cost of space launches to low Earth orbit’, Our World in Data. Accessed: Nov. 30, 2023. [Online]. Available: https://ourworldindata.org/grapher/cost-space-launches-low-earth-orbit
[26] T. Herzig, N. I. Kömle, W. Macher, G. Bihari, and P. Gläser, ‘Site selection, thermodynamics, environment and life support analysis for the PneumoPlanet inflatable lunar habitat concept’, *Planet. Space Sci.*, vol. 224, p. 105595, Dec. 2022, doi: 10.1016/j.pss.2022.105595.
[27] ‘NASA’s Perseverance Mars Rover Extracts First Oxygen from Red Planet - NASA’. Accessed: Nov. 28, 2023. [Online]. Available: https://www.nasa.gov/news-release/nasas-perseverance-mars-rover-extracts-first-oxygen-from-red-planet/
[28] K. Motylinski, M. Wierzbicki, J. Kupecki, and S. Jagielski, ‘Investigation of off-design characteristics of solid oxide electrolyser (SOE) operating in endothermic conditions’, *Renew. Energy*, vol. 170, pp. 277–285, Jun. 2021, doi: 10.1016/j.renene.2021.01.097.
[29] F. Wang *et al.*, ‘Thermodynamic analysis of solid oxide electrolyzer integration with engine waste heat recovery for hydrogen production’, *Case Stud. Therm. Eng.*, vol. 27, p. 101240, Oct. 2021, doi: 10.1016/j.csite.2021.101240.
[30] S. Choi and J. Hong, ‘Versatile thermodynamic design of a solid oxide electrolysis cell system and its sensitivity to operating conditions’, *Energy Convers. Manag.*, vol. 298, p. 117776, Dec. 2023, doi: 10.1016/j.enconman.2023.117776.
[31] Ivar Wærnhus, ‘Mulig tema til Masteroppgaven: SOEC og varmegjenvinning’, Mar. 14, 2023.
[32] R. Balasubramaniam, A. Kashani, R. Grotenrath, and W. Johnson, ‘Gravitational effects on liquefaction systems for Lunar and Mars exploration’, *Cryogenics*, vol. 128, p. 103597, Dec. 2022, doi: 10.1016/j.cryogenics.2022.103597.
[33] W. L. McCabe, J. C. Smith, and P. Harriott, *Unit operations of chemical engineering*, 7. ed., Internat. ed. in McGraw-Hill chemical engineering series. Boston, Mass.: McGraw-Hill Higher Education, 2005.
[34] T. Kuppan, ‘Heat exchanger design handbook’. Taylor & Francis, Boca Raton, 2013.
[35] S. Mahmoudinezhad, M. Sadi, H. Ghiasirad, and A. Arabkoohsar, ‘A comprehensive review on the current technologies and recent developments in high-temperature heat exchangers’, *Renew. Sustain. Energy Rev.*, vol. 183, p. 113467, Sep. 2023, doi: 10.1016/j.rser.2023.113467.
[36] B. Sundén and R. M. Manglik, *Plate Heat Exchangers: Design, Applications and Performance*. WIT Press, 2007.
[37] Q. Li, G. Flamant, X. Yuan, P. Neveu, and L. Luo, ‘Compact heat exchangers: A review and future applications for a new generation of high temperature solar receivers’, *Renew. Sustain. Energy Rev.*, vol. 15, no. 9, pp. 4855–4875, Dec. 2011, doi: 10.1016/j.rser.2011.07.066.
[38] ‘Plate heat exchanger’, *Wikipedia*. Sep. 20, 2023. Accessed: Dec. 12, 2023. [Online]. Available: https://en.wikipedia.org/w/index.php?title=Plate_heat_exchanger&oldid=1176240462
[39] X. Zhang *et al.*, ‘Recent developments in high temperature heat exchangers: A review’, *Front. Heat Mass Transf.*, vol. 11, Jul. 2018, doi: 10.5098/hmt.11.18.
[40] ‘Plate-fin heat exchanger’, *Wikipedia*. Mar. 18, 2023. Accessed: Dec. 12, 2023. [Online]. Available: https://en.wikipedia.org/w/index.php?title=Plate-fin_heat_exchanger&oldid=1145288634

[41] S. Pratheesh Kumar, S. Elangovan, R. Mohanraj, and J. R. Ramakrishna, 'A review on properties of Inconel 625 and Inconel 718 fabricated using direct energy deposition', *Mater. Today Proc.*, vol. 46, pp. 7892–7906, Jan. 2021, doi: 10.1016/j.matpr.2021.02.566.
[42] 'Aspen Exchange Design and Rating'. Aspen tech. Accessed: Dec. 17, 2023. [Windows]. Available: www.aspentech.com/en/products/engineering/aspen-hysys
[43] 'Metals and Alloys - Densities'. Accessed: Dec. 13, 2023. [Online]. Available: https://www.engineeringtoolbox.com/metal-alloys-densities-d_50.html
[44] 'Inconel 625 Tech Data'. Accessed: Dec. 13, 2023. [Online]. Available: https://www.hightempmetals.com/techdata/hitempInconel625data.php
[45] 'Development of large-scale hydrogen liquefaction processes from 1898 to 2009', *Int. J. Hydrog. Energy*, vol. 35, no. 10, pp. 4524–4533, May 2010, doi: 10.1016/j.ijhydene.2010.02.109.
[46] 'High performance, microarchitected, compact heat exchanger enabled by 3D printing', *Appl. Therm. Eng.*, vol. 210, p. 118339, Jun. 2022, doi: 10.1016/j.applthermaleng.2022.118339.

Attachment 1a

Plate Heat Exchanger Specification Sheet

Company:						
Location:						
Service of Unit:	Our Reference:					
Item No.:	Your Reference:H2__first_serrial					
Date: Rev No.:	Job No.:					
CASE		**HOT SIDE**		**COLD SIDE**		
Fluid		Hydrogen		Steam		
Total flow	kg/s	0,0003		0,0012		
Flow per PHE	kg/s	0,0003		0,0012		
Pressure drop (allow./calc.)	bar	0,1 / 0,02077		0,1 / 0,04677		
Velocity between plates	m/s	15,24		13,34		
Wall shear stress	N/m^2	6,99		15,74		
Fouling margin	%					
OPERATING DATA		**INLET**	**OUTLET**	**INLET**	**OUTLET**	
Liquid flow	kg/s	0	0	0	0	
Vapor flow	kg/s	0,0003	0,0003	0,0012	0,0012	
Operating temperature	°C	820	299,11	200	638,51	
Operating pressure	bar	1	0,97923	1	0,95323	
LIQUID PROPERTIES						
Density	kg/m^3					
Specific heat	kJ/(kg-K)					
Viscosity	mPa-s					
Thermal conductivity	W/(m-K)					
Surface tension	N/m					
VAPOR PROPERTIES						
Density	kg/m^3	0,06	0,11	0,46	0,23	
Specific heat	kJ/(kg-K)	6,319	5,88	1,949	2,229	
Viscosity	mPa-s	0,0337	0,0201	0,0164	0,034	
Thermal conductivity	W/(m-K)	0,3834	0,2164	0,0339	0,0848	
Relative molecular mass						
Dew point / bubble point	°C	/		/		
Latent heat	kJ/kg					
Critical pressure	bar	13,13				
Critical temperature	°C	-239,96				
Total heat exchanged	kW	1,1				
Overall coefficient (U)	$W/(m^2-K)$	Clean condition: 138,8		Service: 138,8		
LMTD / Effective MTD	°C	136,17		/ 134,38		
Heat transfer area	m^2	0,1				
Stream heat transfer coeff.	$W/(m^2-K)$	397,2		214,7		
CONFIGURATION FOR EXCHANGER AND PLATE DETAILS						
Number of PHE in parallel		1	Heat transfer area/PHE	m^2	0,1	
Number of passes, hot side		1	Heat transfer area/plate	m^2	0,057	
Number of passes, cold side		1	Plate chevron angles(s)	Degrees	30	
Number of plates per PHE		3	Nominal plate thickness	mm	0,6	
			Nominal plate gap	mm	2,92	
Mass empty / full of water	kg	1,4	/ 1,7			
Remarks:						

Standard 3-plate heat exchanger for serial configuration at 1 bar using hydrogen.

Plate Heat Exchanger Specification Sheet

1	Company:					
2	Location:					
3	Service of Unit:	Our Reference:				
4	Item No.:	Your Reference:H2__first_serrial				
5	Date: Rev No.:	Job No.:				
6	**CASE**		**HOT SIDE**		**COLD SIDE**	
7	Fluid		Hydrogen		Steam	
8	Total flow	kg/s	0,0003		0,0012	
9	Flow per PHE	kg/s	0,0003		0,0012	
10	Pressure drop (allow./calc.)	bar	0,1 / 0,00205		0,1 / 0,00448	
11	Velocity between plates	m/s	1,53		1,26	
12	Wall shear stress	N/m^2	0,69		1,51	
13	Fouling margin	%				
14	**OPERATING DATA**		**INLET**	**OUTLET**	**INLET**	**OUTLET**
15	Liquid flow	kg/s	0	0	0	0
16	Vapor flow	kg/s	0,0003	0,0003	0,0012	0,0012
17	Operating temperature	°C	820	295,61	200	633,65
18	Operating pressure	bar	10	9,99795	10	9,99552
19	**LIQUID PROPERTIES**					
20	Density	kg/m^3				
21	Specific heat	kJ/(kg-K)				
22	Viscosity	mPa-s				
23	Thermal conductivity	W/(m-K)				
24	Surface tension	N/m				
25	**VAPOR PROPERTIES**					
26	Density	kg/m^3	0,57	1,1	4,8	2,4
27	Specific heat	kJ/(kg-K)	6,322	5,893	2,04	2,244
28	Viscosity	mPa-s	0,0337	0,02	0,0165	0,0339
29	Thermal conductivity	W/(m-K)	0,3834	0,2152	0,0339	0,0842
30	Relative molecular mass					
31	Dew point / bubble point	°C	/		/	
32	Latent heat	kJ/kg				
33	Critical pressure	bar	13,13			
34	Critical temperature	°C	-239,96			
35	Total heat exchanged	kW	1,1			
36	Overall coefficient (U)	$W/(m^2-K)$	Clean condition: 138,7		Service: 138,7	
37	LMTD / Effective MTD	°C	135,97		/ 135,48	
38	Heat transfer area	m^2	0,1			
39	Stream heat transfer coeff.	$W/(m^2-K)$	396,4		215	
40	**CONFIGURATION FOR EXCHANGER AND PLATE DETAILS**					
41	Number of PHE in parallel		1	Heat transfer area/PHE	m^2	0,1
42	Number of passes, hot side		1	Heat transfer area/plate	m^2	0,057
43	Number of passes, cold side		1	Plate chevron angles(s)	Degrees	30
44	Number of plates per PHE		3	Nominal plate thickness	mm	0,7
45				Nominal plate gap	mm	2,92
46	Mass empty / full of water	kg	1,6 / 2			
47	Remarks:					
48						
49						
50						

Standard 3-plate heat exchanger for serial configuration at 10 bar using hydrogen.

Plate Heat Exchanger Specification Sheet

1	Company:					
2	Location:					
3	Service of Unit:	Our Reference:				
4	Item No.:	Your Reference:H2__first_serrial				
5	Date: Rev No.:	Job No.:				
6	**CASE**		**HOT SIDE**		**COLD SIDE**	
7	Fluid		Hydrogen		Steam	
8	Total flow	kg/s	0,0003		0,0012	
9	Flow per PHE	kg/s	0,0003		0,0012	
10	Pressure drop (allow./calc.)	bar	0,1 / 0,00916		0,1 / 0,02311	
11	Velocity between plates	m/s	7,62		7	
12	Wall shear stress	N/m^2	1,53		3,86	
13	Fouling margin	%				
14	**OPERATING DATA**		**INLET**	**OUTLET**	**INLET**	**OUTLET**
15	Liquid flow	kg/s	0	0	0	0
16	Vapor flow	kg/s	0,0003	0,0003	0,0012	0,0012
17	Operating temperature	°C	820	208,54	200	706,62
18	Operating pressure	bar	1	0,99084	1	0,97689
19	**LIQUID PROPERTIES**					
20	Density	kg/m^3				
21	Specific heat	kJ/(kg-K)				
22	Viscosity	mPa-s				
23	Thermal conductivity	W/(m-K)				
24	Surface tension	N/m				
25	**VAPOR PROPERTIES**					
26	Density	kg/m^3	0,06	0,13	0,46	0,22
27	Specific heat	kJ/(kg-K)	6,319	5,841	1,949	2,277
28	Viscosity	mPa-s	0,0337	0,0175	0,0164	0,0369
29	Thermal conductivity	W/(m-K)	0,3834	0,1855	0,0339	0,0938
30	Relative molecular mass					
31	Dew point / bubble point	°C	/		/	
32	Latent heat	kJ/kg				
33	Critical pressure	bar	13,13			
34	Critical temperature	°C	-239,96			
35	Total heat exchanged	kW	1,3			
36	Overall coefficient (U)	$W/(m^2-K)$	Clean condition: 82,7		Service: 82,7	
37	LMTD / Effective MTD	°C	40,54 / 37,82			
38	Heat transfer area	m^2	0,4			
39	Stream heat transfer coeff.	$W/(m^2-K)$	235,8		127,9	
40	**CONFIGURATION FOR EXCHANGER AND PLATE DETAILS**					
41	Number of PHE in parallel		1	Heat transfer area/PHE	m^2	0,4
42	Number of passes, hot side		2	Heat transfer area/plate	m^2	0,057
43	Number of passes, cold side		2	Plate chevron angles(s)	Degrees	30
44	Number of plates per PHE		9	Nominal plate thickness	mm	0,6
45				Nominal plate gap	mm	2,92
46	Mass empty / full of water	kg	4,2 / 5,6			
47	Remarks:					
48						
49						
50						

Standard 9-plate heat exchanger for serial configuration at 1 bar using hydrogen.

Plate Heat Exchanger Specification Sheet

1	Company:					
2	Location:					
3	Service of Unit:	Our Reference:				
4	Item No.:	Your Reference:H2__first_serrial				
5	Date: Rev No.:	Job No.:				
6	**CASE**		**HOT SIDE**		**COLD SIDE**	
7	Fluid		Hydrogen		Steam	
8	Total flow	kg/s	0,0003		0,0012	
9	Flow per PHE	kg/s	0,0003		0,0012	
10	Pressure drop (allow./calc.)	bar	0,1 / 0,00019		0,1 / 0,00041	
11	Velocity between plates	m/s	0,38		0,34	
12	Wall shear stress	N/m²	0,06		0,13	
13	Fouling margin	%				
14	**OPERATING DATA**		**INLET**	**OUTLET**	**INLET**	**OUTLET**
15	Liquid flow	kg/s	0	0	0	0
16	Vapor flow	kg/s	0,0003	0,0003	0,0012	0,0012
17	Operating temperature	°C	820	219,17	200	691,06
18	Operating pressure	bar	10	9,99981	10	9,99959
19	**LIQUID PROPERTIES**					
20	Density	kg/m³				
21	Specific heat	kJ/(kg-K)				
22	Viscosity	mPa-s				
23	Thermal conductivity	W/(m-K)				
24	Surface tension	N/m				
25	**VAPOR PROPERTIES**					
26	Density	kg/m³	0,57	1,27	4,8	2,26
27	Specific heat	kJ/(kg-K)	6,322	5,867	2,04	2,282
28	Viscosity	mPa-s	0,0337	0,0178	0,0165	0,0363
29	Thermal conductivity	W/(m-K)	0,3834	0,1892	0,0339	0,0917
30	Relative molecular mass					
31	Dew point / bubble point	°C	/		/	
32	Latent heat	kJ/kg				
33	Critical pressure	bar	13,13			
34	Critical temperature	°C	-239,96			
35	Total heat exchanged	kW	1,2			
36	Overall coefficient (U)	W/(m²-K)	Clean condition: 54,2		Service: 54,2	
37	LMTD / Effective MTD	°C	57,59		/ 56,56	
38	Heat transfer area	m²	0,4			
39	Stream heat transfer coeff.	W/(m²-K)	162,4		81,7	
40	**CONFIGURATION FOR EXCHANGER AND PLATE DETAILS**					
41	Number of PHE in parallel		1	Heat transfer area/PHE	m²	0,4
42	Number of passes, hot side		1	Heat transfer area/plate	m²	0,057
43	Number of passes, cold side		1	Plate chevron angles(s)	Degrees	30
44	Number of plates per PHE		9	Nominal plate thickness	mm	0,7
45				Nominal plate gap	mm	2,92
46	Mass empty / full of water	kg	4,9	/ 6,3		
47	Remarks:					
48						
49						
50						

Standard 9-plate heat exchanger for serial configuration at 10 bar using hydrogen.

Attachment 1b

Plate Heat Exchanger Specification Sheet

1	Company:					
2	Location:					
3	Service of Unit:	Our Reference:				
4	Item No.:	Your Reference:O2_parralel				
5	Date: Rev No.:	Job No.:				
6	**CASE**		**HOT SIDE**		**COLD SIDE**	
7	Fluid		Oxygen		Steam	
8	Total flow	kg/s	0,0008		0,0003	
9	Flow per PHE	kg/s	0,0008		0,0003	
10	Pressure drop (allow./calc.)	bar	0,1 / 0,01979		0,1 / 0,00549	
11	Velocity between plates	m/s	6,11		4,11	
12	Wall shear stress	N/m²	6,66		1,85	
13	Fouling margin	%				
14	**OPERATING DATA**		**INLET**	**OUTLET**	**INLET**	**OUTLET**
15	Liquid flow	kg/s	0	0	0	0
16	Vapor flow	kg/s	0,0008	0,0008	0,0003	0,0003
17	Operating temperature	°C	820	384,31	200	739,64
18	Operating pressure	bar	1	0,98021	1	0,99451
19	**LIQUID PROPERTIES**					
20	Density	kg/m³				
21	Specific heat	kJ/(kg-K)				
22	Viscosity	mPa-s				
23	Thermal conductivity	W/(m-K)				
24	Surface tension	N/m				
25	**VAPOR PROPERTIES**					
26	Density	kg/m³	0,35	0,57	0,46	0,21
27	Specific heat	kJ/(kg-K)	1,102	1,02	1,949	2,301
28	Viscosity	mPa-s	0,0521	0,0372	0,0164	0,0383
29	Thermal conductivity	W/(m-K)	0,0789	0,0523	0,0339	0,0982
30	Relative molecular mass					
31	Dew point / bubble point	°C	/		/	
32	Latent heat	kJ/kg				
33	Critical pressure	bar				
34	Critical temperature	°C				
35	Total heat exchanged	kW	0,4			
36	Overall coefficient (U)	W/(m²-K)	Clean condition: 56		Service: 56	
37	LMTD / Effective MTD	°C	125,22 / 120,48			
38	Heat transfer area	m²	0,1			
39	Stream heat transfer coeff.	W/(m²-K)	127,3		100,2	
40	**CONFIGURATION FOR EXCHANGER AND PLATE DETAILS**					
41	Number of PHE in parallel		1	Heat transfer area/PHE	m²	0,1
42	Number of passes, hot side		1	Heat transfer area/plate	m²	0,057
43	Number of passes, cold side		1	Plate chevron angles(s)	Degrees	30
44	Number of plates per PHE		3	Nominal plate thickness	mm	0,6
45				Nominal plate gap	mm	2,92
46	Mass empty / full of water	kg	1,4 / 1,7			
47	Remarks:					
48						
49						
50						

Standard 3-plate heat exchanger for oxygen parallel configuration at 1 bar.

Plate Heat Exchanger Specification Sheet

1	Company:					
2	Location:					
3	Service of Unit:	Our Reference:				
4	Item No.:	Your Reference:O2_parralel				
5	Date: Rev No.:	Job No.:				
6	**CASE**		**HOT SIDE**		**COLD SIDE**	
7	Fluid		Oxygen		Steam	
8	Total flow	kg/s	0,0008		0,0003	
9	Flow per PHE	kg/s	0,0008		0,0003	
10	Pressure drop (allow./calc.)	bar	0,1 / 0,00196		0,1 / 0,00054	
11	Velocity between plates	m/s	0,61		0,41	
12	Wall shear stress	N/m²	0,66		0,18	
13	Fouling margin	%				
14	**OPERATING DATA**		**INLET**	**OUTLET**	**INLET**	**OUTLET**
15	Liquid flow	kg/s	0	0	0	0
16	Vapor flow	kg/s	0,0008	0,0008	0,0003	0,0003
17	Operating temperature	°C	820	379,69	200	736,84
18	Operating pressure	bar	10	9,99804	10	9,99946
19	**LIQUID PROPERTIES**					
20	Density	kg/m³				
21	Specific heat	kJ/(kg-K)				
22	Viscosity	mPa-s				
23	Thermal conductivity	W/(m-K)				
24	Surface tension	N/m				
25	**VAPOR PROPERTIES**					
26	Density	kg/m³	3,51	5,88	4,8	2,15
27	Specific heat	kJ/(kg-K)	1,103	1,021	2,04	2,313
28	Viscosity	mPa-s	0,0522	0,037	0,0165	0,0382
29	Thermal conductivity	W/(m-K)	0,0789	0,052	0,0339	0,0979
30	Relative molecular mass					
31	Dew point / bubble point	°C	/		/	
32	Latent heat	kJ/kg				
33	Critical pressure	bar				
34	Critical temperature	°C				
35	Total heat exchanged	kW	0,4			
36	Overall coefficient (U)	W/(m²-K)	Clean condition: 55,9		Service: 55,9	
37	LMTD / Effective MTD	°C	125,29 / 121,99			
38	Heat transfer area	m²	0,1			
39	Stream heat transfer coeff.	W/(m²-K)	127,1		100,2	
40	**CONFIGURATION FOR EXCHANGER AND PLATE DETAILS**					
41	Number of PHE in parallel		1	Heat transfer area/PHE	m²	0,1
42	Number of passes, hot side		1	Heat transfer area/plate	m²	0,057
43	Number of passes, cold side		1	Plate chevron angles(s)	Degrees	30
44	Number of plates per PHE		3	Nominal plate thickness	mm	0,7
45				Nominal plate gap	mm	2,92
46	Mass empty / full of water	kg	1,6 / 2			
47	Remarks:					
48						
49						
50						

Standard 3-plate heat exchanger for oxygen parallel configuration at 10 bar.

Attachment 1c

Plate Heat Exchanger Specification Sheet

1	Company:					
2	Location:					
3	Service of Unit:	Our Reference:				
4	Item No.:	Your Reference:O2_parralel				
5	Date: Rev No.:	Job No.:				
6	**CASE**		**HOT SIDE**		**COLD SIDE**	
7	Fluid		Oxygen		Steam	
8	Total flow	kg/s	0,0008		0,0003	
9	Flow per PHE	kg/s	0,0008		0,0003	
10	Pressure drop (allow./calc.)	bar	0,1 / 0,01265		0,1 / 0,00425	
11	Velocity between plates	m/s	3,05		2,21	
12	Wall shear stress	N/m²	2,12		0,71	
13	Fouling margin	%				
14	**OPERATING DATA**		**INLET**	**OUTLET**	**INLET**	**OUTLET**
15	Liquid flow	kg/s	0	0	0	0
16	Vapor flow	kg/s	0,0008	0,0008	0,0003	0,0003
17	Operating temperature	°C	820	313,12	200	815,58
18	Operating pressure	bar	1	0,98735	1	0,99575
19	**LIQUID PROPERTIES**					
20	Density	kg/m³				
21	Specific heat	kJ/(kg-K)				
22	Viscosity	mPa-s				
23	Thermal conductivity	W/(m-K)				
24	Surface tension	N/m				
25	**VAPOR PROPERTIES**					
26	Density	kg/m³	0,35	0,65	0,46	0,2
27	Specific heat	kJ/(kg-K)	1,102	0,999	1,949	2,354
28	Viscosity	mPa-s	0,0521	0,0343	0,0164	0,0415
29	Thermal conductivity	W/(m-K)	0,0789	0,0475	0,0339	0,1087
30	Relative molecular mass					
31	Dew point / bubble point	°C	/		/	
32	Latent heat	kJ/kg				
33	Critical pressure	bar				
34	Critical temperature	°C				
35	Total heat exchanged	kW	0,4			
36	Overall coefficient (U)	W/(m²-K)	Clean condition: 39,4		Service: 39,4	
37	LMTD / Effective MTD	°C	33,51 / 28,35			
38	Heat transfer area	m²	0,4			
39	Stream heat transfer coeff.	W/(m²-K)	82,4		75,8	
40	**CONFIGURATION FOR EXCHANGER AND PLATE DETAILS**					
41	Number of PHE in parallel		1	Heat transfer area/PHE	m²	0,4
42	Number of passes, hot side		2	Heat transfer area/plate	m²	0,057
43	Number of passes, cold side		2	Plate chevron angles(s)	Degrees	30
44	Number of plates per PHE		9	Nominal plate thickness	mm	0,6
45				Nominal plate gap	mm	2,92
46	Mass empty / full of water	kg	4,2 / 5,6			
47	Remarks:					
48						
49						
50						

Standard 9-plate heat exchanger for oxygen parallel configuration at 1 bar.

Plate Heat Exchanger Specification Sheet

1	Company:					
2	Location:					
3	Service of Unit:	Our Reference:				
4	Item No.:	Your Reference:O2_parralel				
5	Date: Rev No.:	Job No.:				
6	**CASE**		**HOT SIDE**		**COLD SIDE**	
7	Fluid		Oxygen		Steam	
8	Total flow	kg/s	0,0008		0,0003	
9	Flow per PHE	kg/s	0,0008		0,0003	
10	Pressure drop (allow./calc.)	bar	0,1 / 0,00125		0,1 / 0,00042	
11	Velocity between plates	m/s	0,31		0,22	
12	Wall shear stress	N/m²	0,21		0,07	
13	Fouling margin	%				
14	**OPERATING DATA**		**INLET**	**OUTLET**	**INLET**	**OUTLET**
15	Liquid flow	kg/s	0	0	0	0
16	Vapor flow	kg/s	0,0008	0,0008	0,0003	0,0003
17	Operating temperature	°C	820	306,07	200	815,1
18	Operating pressure	bar	10	9,99875	10	9,99958
19	**LIQUID PROPERTIES**					
20	Density	kg/m³				
21	Specific heat	kJ/(kg-K)				
22	Viscosity	mPa-s				
23	Thermal conductivity	W/(m-K)				
24	Surface tension	N/m				
25	**VAPOR PROPERTIES**					
26	Density	kg/m³	3,51	6,63	4,8	1,99
27	Specific heat	kJ/(kg-K)	1,103	1	2,04	2,365
28	Viscosity	mPa-s	0,0522	0,0341	0,0165	0,0415
29	Thermal conductivity	W/(m-K)	0,0789	0,047	0,0339	0,1086
30	Relative molecular mass					
31	Dew point / bubble point	°C	/		/	
32	Latent heat	kJ/kg				
33	Critical pressure	bar				
34	Critical temperature	°C				
35	Total heat exchanged	kW	0,5			
36	Overall coefficient (U)	W/(m²-K)	Clean condition: 39,3		Service: 39,3	
37	LMTD / Effective MTD	°C	32,91 / 28,87			
38	Heat transfer area	m²	0,4			
39	Stream heat transfer coeff.	W/(m²-K)	82,2		75,5	
40	**CONFIGURATION FOR EXCHANGER AND PLATE DETAILS**					
41	Number of PHE in parallel		1	Heat transfer area/PHE	m²	0,4
42	Number of passes, hot side		2	Heat transfer area/plate	m²	0,057
43	Number of passes, cold side		2	Plate chevron angles(s)	Degrees	30
44	Number of plates per PHE		9	Nominal plate thickness	mm	0,7
45				Nominal plate gap	mm	2,92
46	Mass empty / full of water	kg	4,9 / 6,3			
47	Remarks:					
48						
49						
50						

Standard 9-plate heat exchanger for oxygen parallel configuration at 10 bar.

PLATE-FIN Heat Exchanger Specification Sheet

2	Company:													
3	Location:													
4	Service of Unit:				Our Reference:									
5	Item No.:				Your Reference:									
6	Date:			Rev No.:	Job No.:									
7	Stream i.d./fluid name				1/			2/			3/			
8	Flow rate	Total		kg/s	0,0008			0,0003			0,0012			
9		Vap./liq.	In	kg/s	0,0008	/	0	0,0003	/	0	0,0012	/	0	
10		Vap./liq.	Out		0,0008	/	0	0,0003	/	0	0,0012	/	0	
11	Molecular weight	Vap.	In/Out		31,9988	/	31,9988	5,21576	/	5,21576	18,01528	/	18,01528	
12		Liq.	In/Out			/			/			/		
13	Density	Vap.	In/Out	kg/m³	0,35	/	0,44	0,06	/	0,07	0,46	/	0,22	
14		Liq.	In/Out			/			/			/		
15	Viscosity	Vap.	In/Out	mPa-s	0,0521	/	0,0415	0,0337	/	0,0256	0,0164	/	0,0322	
16		Liq.	In/Out			/			/			/		
17	Specific heat	Vap.	In/Out	kJ/(kg-K)	1,102	/	1,049	6,319	/	6	1,94	/	2,197	
18		Liq.	In/Out			/			/			/		
19	Thermal cond.	Vap.	In/Out	W/(m-K)	0,0789	/	0,0597	0,3834	/	0,2825	0,0339	/	0,0792	
20		Liq.	In/Out			/			/			/		
21	Temperature		In/Out	°C	820	/	500	820	/	500	200	/	594,94	
22	Operating pressure		In	bar	1			1			1			
23	Maximum allowable pressure drop			bar	0,2			0,2			0,2			
24	Heat load			kW	-0,3			-0,7			1			
25	Calculated MTD			°C	258,01									
26	Fouling resistance			m²-K/W	0			0			0			
27	Core size			mm	Width		45,09	Height		27,3	Length		268,55	
28	Number of layers				1			1			1			
29	Fin code: Heat transfer fin				1			1			1			
30	Fin code: Distributor fin				2			2			2			
31	Heat transfer surface/core			m²	0			0			0			
32	Core opening size		In/Out	mm	7,95	/	7,95	7,95	/	7,95	29,6	/	29,6	
33	Nozzle size		In/Out	mm	26,64	/	26,64	26,64	/	26,64	26,64	/	26,64	
34	Calculated frictional pressure drop			bar	0,04355			0,06297			0,04111			
35	Notes													
36														
37														

Plate-fin with a design input of 500˚C (target outlet temperature of the hot streams).

PLATE-FIN Heat Exchanger Specification Sheet

2	Company:													
3	Location:													
4	Service of Unit:			Our Reference:										
5	Item No.:			Your Reference:										
6	Date:		Rev No.:	Job No.:										
7	Stream i.d./fluid name				1/			2/			3/			
8	Flow rate	Total		kg/s	0,0008			0,0003			0,0012			
9		Vap./liq.	In	kg/s	0,0008	/	0	0,0003	/	0	0,0012	/	0	
10		Vap./liq.	Out		0,0008	/	0	0,0003	/	0	0,0012	/	0	
11	Molecular weight	Vap.	In/Out		31,9988	/	31,9988	5,21576	/	5,21576	18,01528	/	18,01528	
12		Liq.	In/Out			/			/			/		
13	Density	Vap.	In/Out	kg/m³	0,35	/	0,49	0,06	/	0,08	0,46	/	0,23	
14		Liq.	In/Out			/			/			/		
15	Viscosity	Vap.	In/Out	mPa-s	0,0521	/	0,0409	0,0337	/	0,0249	0,0164	/	0,0333	
16		Liq.	In/Out			/			/			/		
17	Specific heat	Vap.	In/Out	kJ/(kg-K)	1,102	/	1,045	6,319	/	5,981	1,94	/	2,214	
18		Liq.	In/Out			/			/			/		
19	Thermal cond.	Vap.	In/Out	W/(m-K)	0,0789	/	0,0586	0,3834	/	0,275	0,0339	/	0,0824	
20		Liq.	In/Out			/			/			/		
21	Temperature		In/Out	°C	820	/	483,2	820	/	476,68	200	/	619,82	
22	Operating pressure		In	bar	1			1			1			
23	Maximum allowable pressure drop			bar	0,2			0,2			0,2			
24	Heat load			kW	-0,3			-0,7			1			
25	Calculated MTD			°C	233,24									
26	Fouling resistance			m²-K/W	0			0			0			
27	Core size			mm	Width		45,09	Height		27,3	Length		268,69	
28	Number of layers				1			1			1			
29	Fin code: Heat transfer fin				3			3			3			
30	Fin code: Distributor fin				2			2			2			
31	Heat transfer surface/core			m²	0			0			0			
32	Core opening size		In/Out	mm	7,95	/	7,95	7,95	/	7,95	29,6	/	29,6	
33	Nozzle size		In/Out	mm	26,64	/	26,64	26,64	/	26,64	26,64	/	26,64	
34	Calculated frictional pressure drop			bar	0,04035			0,05764			0,03759			
35	Notes													
36														
37														

Plate-fin with a design input of 400˚C (target outlet temperature of the hot streams).


UNIVERSITAS
BERGENSIS


Høgskulen
på Vestlandet